Chapter 6

Mass Fitting

The goal of this chapter is to develop the tools needed to reconstruct the top mass in a $t\bar{t} \to l + \text{jets}$ decay. Unfortunately, there is not a unique prescription for accomplishing this; further, there are relatively large, mass-dependent biases which are difficult to eliminate. Therefore, the quantity which will be constructed is best thought of not as *the* top mass for an event, but rather as merely an observable which is correlated with the top mass. In order to distinguish the two, the result of this procedure will be referred to as the 'fitted' mass. The final stage of the analysis (discussed in Chapter 7) will go from fitted masses to the final top mass.

Further information on mass fitting at DØ may be found in [98, 136].

6.1 Introduction

Here is a summary of the steps used in constructing the fitted mass. The points raised here will be expanded on later in this chapter.

- The inputs to the analysis are the kinematic parameters of the lepton, jets, and missing E_T in the event.

- To reduce the confusion caused when multiple partons get merged together in a single jet, the relatively narrow cone size of $R = 0.3$ is used. As mentioned in Section 4.5.2, the standard MPF jet corrections do not fully account for out-of-cone radiation, so an additional correction needs to be made (see Section 6.2.1). Jets with a muon tag receive an extra correction to account for the energy carried off by the muon and neutrino.

- Jets are required to have $|\eta| < 2.5$ and $E_T > 15\,\mathrm{GeV}$ (after all corrections). There must be at least four such jets in an event in order to start the fit; events with fewer jets are discarded. Only the four jets with the highest E_T are used in the fit.

- If the correspondence between jets and partons were known, one could simply sum them up in the appropriate combinations to obtain the masses of the two tops. But in general, this is not known. Instead, all twelve possible assignments of the four jets are tried and only the 'best' solutions are retained.

- But how to quantify 'best'? Recall from Section 2.4 that the system is overconstrained by two equations. One can thus define a χ^2 which tells how far the kinematic parameters of the event must be pulled from their measured values in order for the constraints to be satisfied. The 'best' permutations are then the ones with the lowest χ^2 values. The results of this kinematic fit can also be used to define an improved value for the top mass.

- Finally, the fitted mass of an event is defined as the χ^2-weighted average of (up to) the best three jet permutations which satisfy a loose χ^2 cut of $\chi^2 < 7$. If the event contains a tagged jet, a jet permutation is considered only if it assigns the tagged jet as a b jet.

6.2 Final Jet Corrections

6.2.1 Out-Of-Cone Correction

Following the MPF jet corrections (see Section 4.5.2), an additional correction is applied. The intent of this correction is to account for radiation outside of the jet cone; it attempts to make the jet energies match those of the original partons. It was derived by looking at an ISAJET $t\bar{t}$ Monte Carlo sample and comparing the energies of the MPF-corrected reconstructed jets with the energies of the partons which most nearly match those jets. (The ISAJET `ISAQ` partons were used, i.e., after QCD evolution but before fragmentation.) The correction is a simple linear form [98]:

$$E_T(\mathrm{corr}) = 5.556 + 1.087 E_T(\mathrm{MPF}) \tag{6.1}$$

(for $R = 0.3$ cone jets).

Figure 6.1 shows the reconstructed mass of the hadronic W in ISAJET top events, after the full detector simulation and reconstruction, both before and after the out-of-cone corrections. (ISAJET parton-ID information was used to find the jets resulting from the decay of the W. All such jets satisfying $E_T > 15\,\text{GeV}$ and $|\eta| < 2$ are used, not just those in the highest four E_T jets.) It can readily be seen the the correction moves the distribution much closer to the true W mass.

As an additional check, one can look at $(Z \to ee) + 1$ jet events. In these events, the Z is well-measured, and should be balanced in the transverse plane by the single jet. Figure 6.2 shows the difference between the electron pair and jet transverse energies for data and Monte Carlo both before and after the out-of-cone correction. One sees that there is good agreement between the data and the Monte Carlo, and also that the corrections significantly reduce the transverse momentum imbalance between the electron pair and the jet.

The Z data are also used to estimate the systematic error on the jet energy scale, including the out-of-cone corrections. A clean sample of $(Z \to ee)+1$ jet events is selected. Events with more than one ($R = 0.3$ cone) jet are excluded from the sample (with no E_T cut on the jet). Define the quantity f as

$$f = \frac{E_T(\text{jet}) - E_T(ee)}{E_T(ee)}. \tag{6.2}$$

An upper limit on the energy scale error is then estimated by computing the absolute value of the mean of f and its error, and adding these two numbers in quadrature. The results are as follows [137].

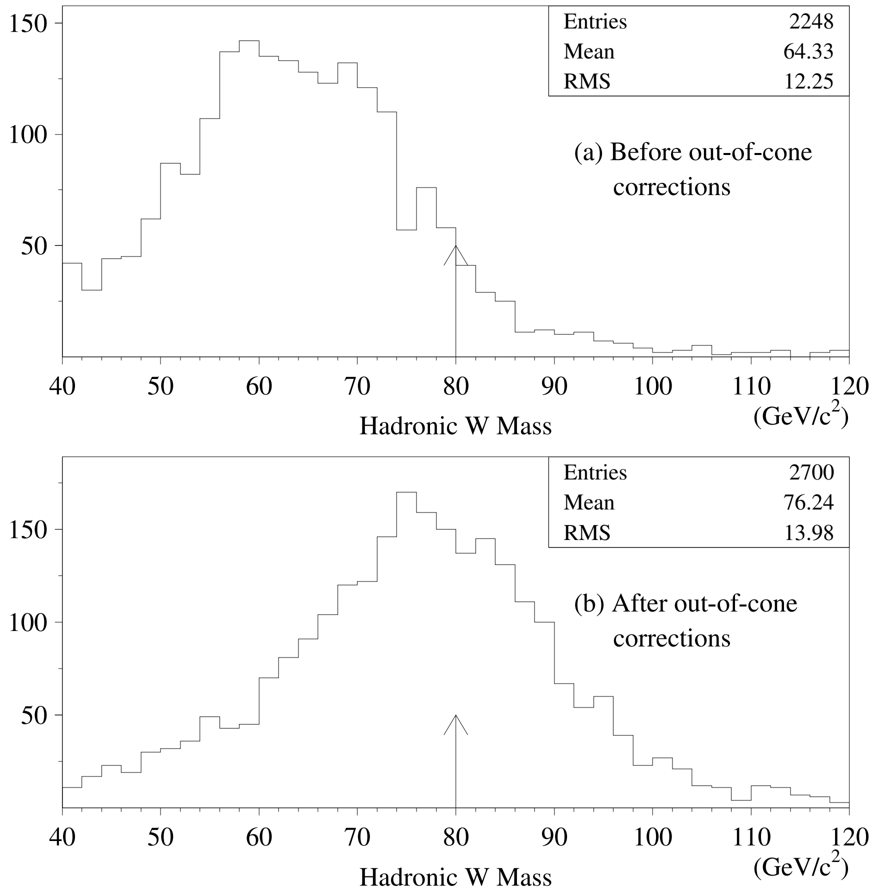

Figure 6.1: Reconstructed hadronic W mass, (a) before and (b) after out-of-cone corrections (using $R = 0.3$ cone jets). From ISAJET 180 GeV/c^2 $t\bar{t}$ Monte Carlo, using all jets which were actually from W decay and with $E_T > 15$ GeV and $|\eta| < 2$.

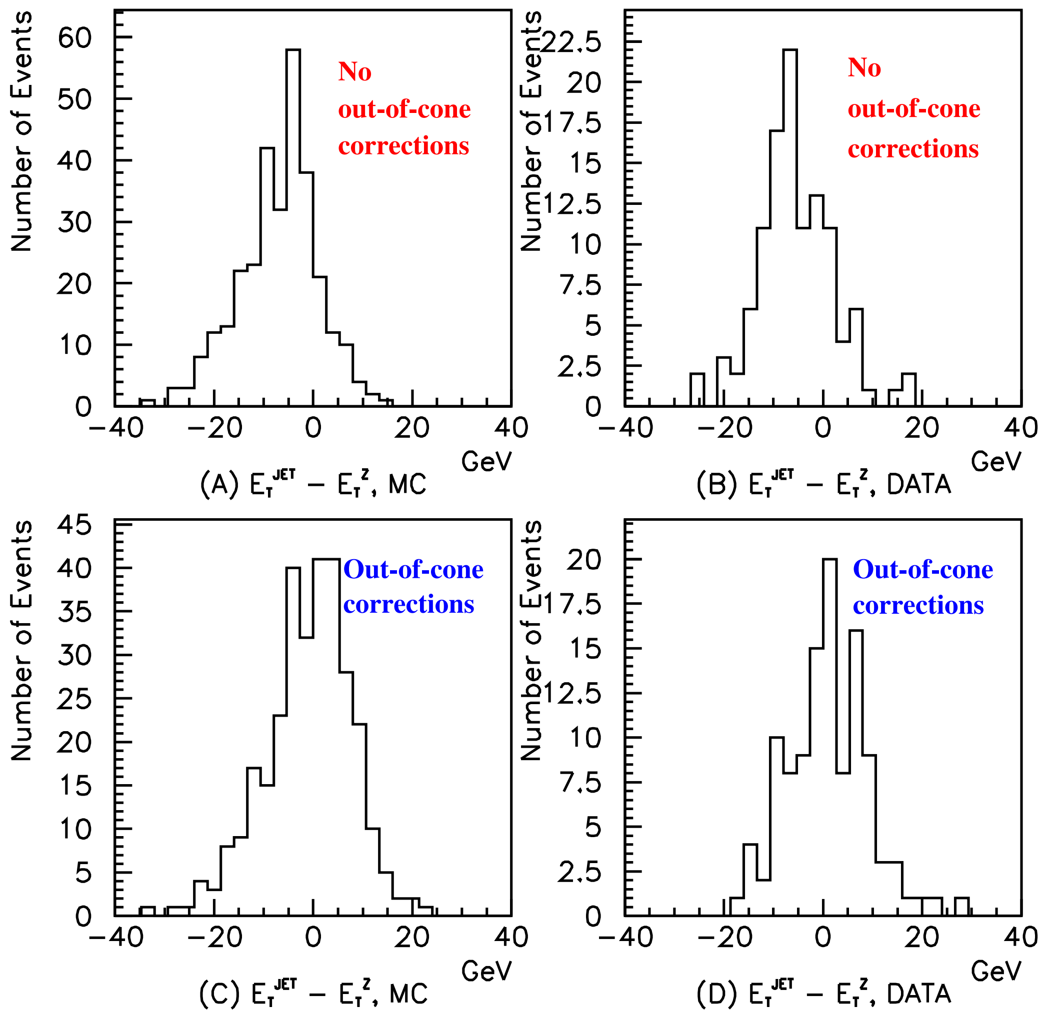

Figure 6.2: Difference between the transverse momenta of the electron pair and the jet in $(Z \rightarrow ee) + 1$ jet events. For Monte Carlo and data, with and without out-of-cone corrections. [98, p. 61]

$E_T(Z)$	$\lvert\langle f\rangle\rvert$	Error on $\lvert\langle f\rangle\rvert$	Estimate of jet scale error
10–20 GeV	0.3	0.06	30%
20–30 GeV	0.004	0.05	5.0%
30–40 GeV	0.06	0.05	7.8%
40–50 GeV	0.023	0.08	8.6%
$>$ 50 GeV	0.018	0.07	7.0%

The lowest energy band is somewhat anomalous, but most jets in top events have higher transverse energies. Thus, an upper limit on the error on jet energy scale is estimated to be about 10%.

For further details about the out-of-cone corrections, see [98, pp. 55–61].

6.2.2 Tagged Jet Correction

For jets which have a muon tag, there is one further correction which should be made. These jets presumably came from a b which underwent a semileptonic decay into a muon and a neutrino. To get back the momentum of the original b, the momenta of both the muon and the neutrino should be added into the jet. Of course, the momentum of the neutrino is not measured, but as Figure 6.3 shows, adding twice the muon momentum to the jet is a reasonable approximation.

6.3 Fitting Algorithm

Now that the jet corrections are sorted out, the kinematic fitting algorithm itself can be examined.

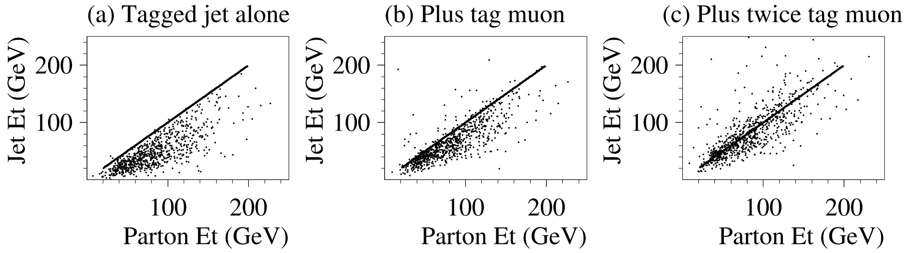

Figure 6.3: Comparison of transverse energies of reconstructed tagged jets (vertical axis) to matched partons (horizontal axis). (a) No tagging correction. (b) Tag muon momentum added to the tagged jet. (c) Twice the tag muon momentum added to the tagged jet. From ISAJET 180 GeV/c^2 $t\bar{t}$ Monte Carlo.

6.3.1 Fit Variables

The first thing to do is to define the variables which will be used in the fit. It is convenient to choose them so that they are as uncorrelated as possible.

For the lepton and each jet, there are three measured variables: its energy (or momentum), and its direction (which is a two dimensional quantity). The variables which will be used to describe an electron or jet are its momentum p, azimuthal angle ϕ, and pseudorapidity η. Muons are described in a similar manner, except that instead of p, the inverse momentum $k = 1/p$ is used, since the errors are more nearly gaussian in that variable. The masses of the jets are fixed to zero, except for the jets which are assigned as b-jets, which are given masses of 5 GeV/c^2. (This is done by taking the momentum components of the jet as the measurement, and changing the energy component of the four-vector to set the desired mass. Since these masses are small compared to the typical jet energies (> 15 GeV), the exact prescription used doesn't make much difference for the final result. For another method of dealing with jet masses, see [98].)

To represent the transverse momentum of the neutrino, one could use the x and y components of the missing E_T. However, that is not ideal, since the missing E_T is highly correlated with all the other energy measurements: a fluctuation in jet measurement will show up as an exactly corresponding fluctuation in the missing E_T. A better quantity is k_T, which is defined as

$$\vec{k_T} = \vec{E}_T(\text{lep}) + \vec{\not{E}}_T + \sum_{i \in \text{jets}} \vec{E}_T(\text{jet}_i). \tag{6.3}$$

The sum over jets here includes only jets assumed to be part of the final state. This variable can be interpreted as the transverse momentum of the $t\bar{t}$ system (it is the negation of the 'baby jet' of [98]). The x and y components of $\vec{k_T}$ are used as fit variables.

There is one remaining variable, which is taken to be the z-component of the neutrino momentum. This gives a total of eighteen variables (for four jets).

Each measured variable still needs to have an error attached to it; this will be discussed later. All the errors are assumed to be uncorrelated (i.e., a diagonal error matrix).

6.3.2 Jet Permutations

As mentioned above, a fit is tried for each possible jet permutation. For four jets, there are twelve such permutations: there are twenty-four permutations of four objects, but the two jets which are assigned to the hadronic W

can be interchanged without changing the solution, so only twelve of them are distinct.

Before attempting a fit, loose cuts are made to reject permutations which are likely to yield poor fits. The hadronic W mass, before fitting, is required to be within the range $40\,\mathrm{GeV}/c^2 < m_W < 120\,\mathrm{GeV}/c^2$. In addition, permutations which have a large value for the smallest solution for the z-component of the neutrino momentum (see Section 6.3.3 and Appendix B) are rejected.

For future reference, consider the problem of jet permutations for more than four jets. There are two possibilities for dealing with an extra jet: it can be considered initial state radiation (ISR) and dropped from the problem, or it can be considered to have been radiated from one of the final state partons (final-state radiation, or FSR), in which case it should be merged with the appropriate jet. Due to interference terms in the production and decay matrix elements, this separation into ISR and FSR is only an approximation, but it works reasonably well for radiation which is large enough to be seen as a separate jet [138].

In combinatorial terms, the problem can be stated as follows. Find all distinct ways of tagging N objects with the labels

- b_l, for the leptonic-side b,
- b_h, for the hadronic-side b,
- w, for the decay products of the hadronic W, and
- i, for initial state radiation,

subject to the conditions that there be at least one b_l, one b_h, and two w's. The number of such permutations grows extremely rapidly with N; the first few values are as follows:

$$\begin{array}{lr} N=4 & 12 \\ N=5 & 140 \\ N=6 & 1020 \\ N=7 & 5992 \end{array}$$

This combinatorial explosion is one of the main motivations for restricting the fit to just the top four jets.

6.3.3 Constrained Fit

The constrained fit itself can now be described. Form the fit variables into a one-dimensional vector $\mathbf{x}$, and define a χ^2 by

$$\chi^2 = (\mathbf{x} - \mathbf{x}^m)^T \mathbf{G} (\mathbf{x} - \mathbf{x}^m), \tag{6.4}$$

where $\mathbf{x}$ is the vector of fit variables, $\mathbf{x}^m$ is the vector of the measured values of those variables, and $\mathbf{G}$ is the inverse error matrix. This quantity should be minimized subject to the constraints

$$m_{W_{\rm lep}} = 80.2\,{\rm GeV}/c^2 \tag{6.5}$$

$$m_{W_{\rm had}} = 80.2\,{\rm GeV}/c^2 \tag{6.6}$$

$$m_t = m_{\bar{t}}. \tag{6.7}$$

Were these constraints linear in the fit variables, the problem would be exactly solvable using the method of Lagrange multipliers and simple linear algebra.

Unfortunately, that is not the case. Instead, an iterative technique is used. Starting at the point given by the measured values of the variables, The constraint equations are expanded in a power series around this point to linearize them, and the minimization is solved with these linearized constraints. This result defines the starting point for the next minimization step, and the iteration continues until the constraints are satisfied and the χ^2 stops changing. Further details on the fitting method may be found in Appendix A.

There is one additional wrinkle to this procedure. To start the above procedure, one must specify an initial value for *all* variables — not just the measured ones. In particular, a starting value is needed for the z-component of the neutrino momentum, p_z^ν. This is done by choosing it such that the two tops have equal mass. This yields the following quadratic equation for p_z^ν:

$$\left((p_z^c)^2 - (E^c)^2\right)(p_z^\nu)^2 + \alpha p_z^c p_z^\nu - (E^c {p_T}^\nu)^2 + \alpha^2/4 = 0, \tag{6.8}$$

where

$$\alpha = m_t^2 - m_c^2 + 2\vec{p_T}^\nu \cdot \vec{p_T}^c, \tag{6.9}$$

and the four-vector c is the sum of the four-vectors of the lepton and b-jet. If the solutions are complex, the real part is used. Otherwise, there will be two real solutions. Both are tried, and the fit with the lowest χ^2 is retained.

Note that since p_z^ν does not enter into the χ^2 (since its measurement error is effectively infinite), the only effect it can have on the final answer is to influence which local minimum the fit will find, if there happen to be more than one. Only in about 10–20% of top events do two distinct neutrino solutions yield different fit results.

6.3.4 Solution Averaging

The procedure so far gives a set of (χ^2, fitted mass) pairs, one for each jet permutation which was successfully fit. However, it would be most convenient to be able to represent the result of the fit by a single number. One way of doing this would be to pick the solution which has the best χ^2. This has the drawback, however, that this value can undergo large, discontinuous changes for small changes in the input parameters, as the χ^2 values change and different permutations come to have the smallest χ^2. On the other hand, the result should not depend strongly on fits which have a relatively poor χ^2. An additional observation is that while there is at most one 'correct' jet permutation in an event (and it rarely turns out to have the best χ^2), there are several additional 'semicorrect' permutations (where the jets are assigned to the proper tops) which contain nearly as much mass information as the correct permutation.

Therefore, a compromise is to take the weighted average of the best few solutions, where the weight is taken to be $e^{-\chi^2/2}$. For this analysis, a loose χ^2 cut is imposed ($\chi^2 < 7$), and the weighted average of the fitted masses for the three best solutions is used (or however many good solutions there are, if this number is less than three). If the event has a tagged jet, the only permutations used in the average are those in which the tagged jet was used as a b.

6.4 Parton-Level Tests

The first tests of the fitter will use parton-level results from the ISAJET Monte Carlo [120]. Here, 'parton-level' means the results from ISAJET following the QCD evolution phase, but before fragmentation (the '`ISAQ`' particles). No detector simulation is included. To (crudely) model the effects of the jet-finding algorithm, partons are grouped together inside of cones of radius $R = 0.45$. The resulting objects, called 'pjets' [139], are then treated as jets.

Unless otherwise stated, the data were smeared with gaussians with the widths given in the following table.

$\frac{\sigma E(e)}{E(e)} = \frac{0.18\sqrt{\mathrm{GeV}}}{\sqrt{E}}$	$\frac{\sigma E(\mathrm{jet})}{E(\mathrm{jet})} = \frac{1.19\sqrt{\mathrm{GeV}}}{\sqrt{E}}$	
$\sigma\phi(e) = 0.0060\,\mathrm{rad}$	$\sigma\phi(\mathrm{jet}) = 0.035\,\mathrm{rad}$	(6.10)
$\sigma\eta(e) = 0.0072$	$\sigma\eta(\mathrm{jet}) = 0.040$	
$\sigma k_{Tx} = 12\,\mathrm{GeV}$	$\sigma k_{Ty} = 12\,\mathrm{GeV}$	

These same numbers are used for the object resolutions in the constrained fit.

The parton-level studies are restricted to the $e + \mathrm{jets}$ channel. The kinematic cuts applied are the same as used for the data analysis:

$$\begin{array}{ll} E_T(e) > 20\,\mathrm{GeV} & |\eta(e)| < 2 \\ E_T(\mathrm{jet}) > 15\,\mathrm{GeV} & |\eta(\mathrm{jet})| < 2 \\ \not{E}_T > 25\,\mathrm{GeV}. & \end{array} \tag{6.11}$$

The four jets with the largest E_T within $|\eta| < 2.5$ are selected for use in the fit. For these parton-level studies, a χ^2 cut of $\chi^2 < 20$ is required of all fits.

To start with, examine Figure 6.4(a). This shows the result of fitting an unsmeared $t\bar{t}$ Monte Carlo sample with $m_t = 180\,\mathrm{GeV}/c^2$. The unshaded

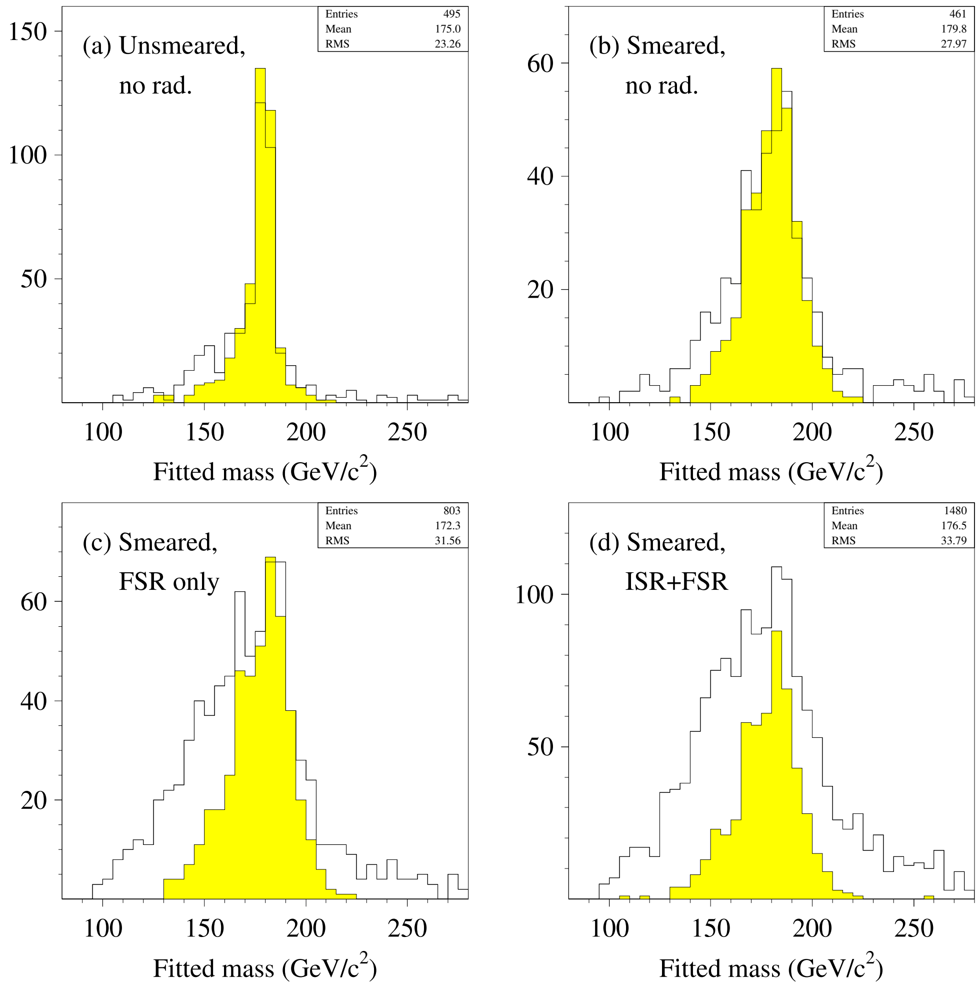

Figure 6.4: Results of fits with a $t\bar{t} \to e+$jets parton-level ISAJET Monte Carlo with $m_t = 180\,\mathrm{GeV}/c^2$, for different radiation conditions. The unshaded plot is the jet permutation with the smallest χ^2, and the shaded plot is the correct jet permutation. (a) Unsmeared, no radiation (see text). (b) Smeared, no radiation. (c) Smeared, FSR only. (d) Smeared, ISR and FSR. For all plots, the fit χ^2 was required to be less than 20. Statistics reflect the unshaded plot.

histogram is the jet permutation with the smallest χ^2 and the shaded histogram is the correct jet permutation. (Note that for any given event, the result from the correct permutation will usually be different than that from the best permutation. Thus, although the events appearing in the shaded plots are a subset of those in the unshaded plots, the shaded plots do not necessarily lie completely beneath the unshaded ones.) For this plot, the sample was further filtered to remove events containing significant radiation, either initial-state (ISR) or final state (FSR). More precisely, events were required to have exactly four jets which correspond to the four primary partons. The distributions peak in nearly the right place, but there is a small tail on the low end caused by residual radiation. Another factor which contributes to the width of these plots is the fact that the W masses are generated from a Breit-Wigner distribution, while the fit always forces the W masses to a constant value.

Continuing, Figure 6.4(b) shows what happens when smearing is turned on. In Figure 6.4(c), events are allowed to have significant final state radiation, but events with significant initial state radiation are still filtered out. This increases the low-end tail, since energy gets lost when one picks just the top four jets in an event with FSR. Finally, in Figure 6.4(d), there is no filtering out of radiation. This inclusion of ISR increases the tail at the high end, but also brings the means of the distributions back towards the input mass.

The χ^2 distribution for this sample (with full radiation) is shown in Figure 6.5, for the first three lowest χ^2 fits and the correct permutation. The distribution of correct fits peaks at zero, as it should, while those from the

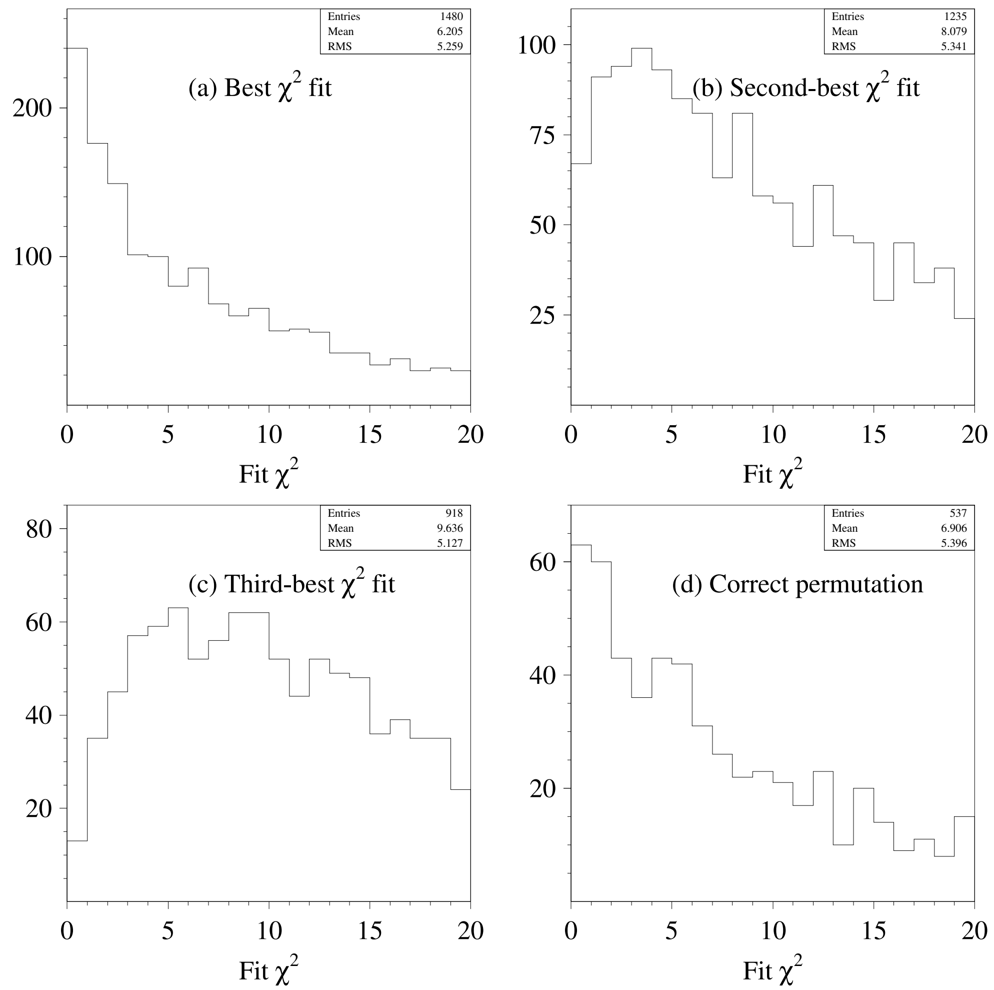

Figure 6.5: Fit χ^2 distributions for (a) best, (b) second-best, and (c) third-best χ^2 solutions and (d) the correct jet permutation. For smeared parton-level $t\bar{t} \to e + \text{jets}$ ISAJET Monte Carlo,with $m_t = 180\,\text{GeV}/c^2$.

second- and third-best fits start to peak away from zero. Note, however, that even though the resolutions used for the fit are the same as were used for smearing the data, the mean of the χ^2 distribution for the correct permutations is rather larger than one would expect (2, for a 2C fit). This is again due to the effects of radiation and the non-zero widths of the W's. For fits using the full detector simulation, these effects will get absorbed into the object resolutions.

As mentioned in Section 6.3.4, what is actually used as the result from the fit is not the best χ^2 solution, but instead a weighted average of up to the three best solutions. (The weight used is the χ^2 probability $e^{-\chi^2/2}$.) Figure 6.6 shows the mass distributions that result from using the best, second-best, and third-best χ^2 permutations, as well as the weighted average of the three. As the χ^2 values go up, the resulting mass values tend to be biased low. The weighted average, however, is not biased, and is slightly narrower than the result of using the best χ^2 solution.

Figure 6.7 shows the effect of varying the amount of jet smearing. As the amount of smearing increases, the widths of the distributions increase, as expected, although the increase is rather gradual. Also note that as the smearing is increased, the distributions remain centered at the correct value.

Figure 6.8 shows effect of scaling the energies of all the jets up or down by the 10% estimated systematic error in the jet energy scale (see Section 6.2.1). This translates into a change in the fitted mass of about 10 GeV in either direction, or $\approx 5.5\%$.

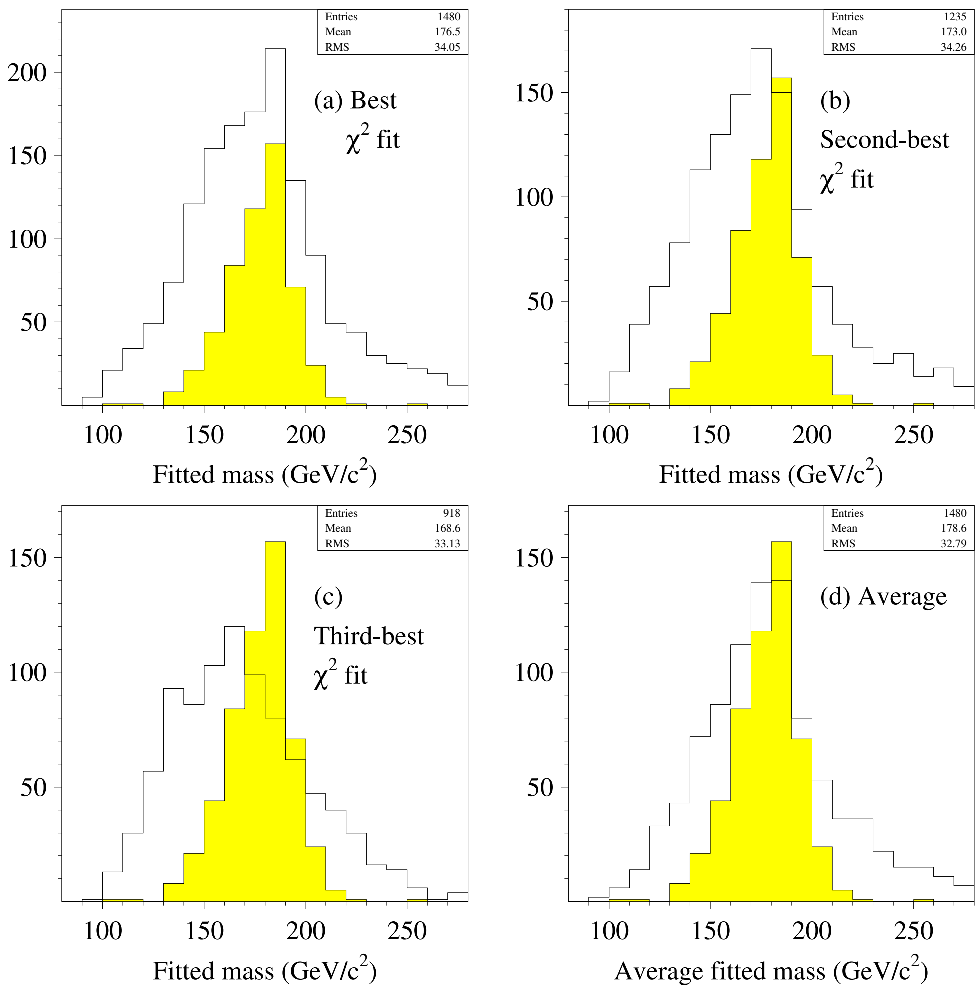

Figure 6.6: Fitted mass distributions for (a) best, (b) second-best, and (c) third-best χ^2 solutions and (d) weighted average. For smeared $t\bar{t} \rightarrow e$+jets ISAJET Monte Carlo with $m_t = 180\,\mathrm{GeV}/c^2$. Shaded plots show the result for the correct jet permutation (the same for all four plots).

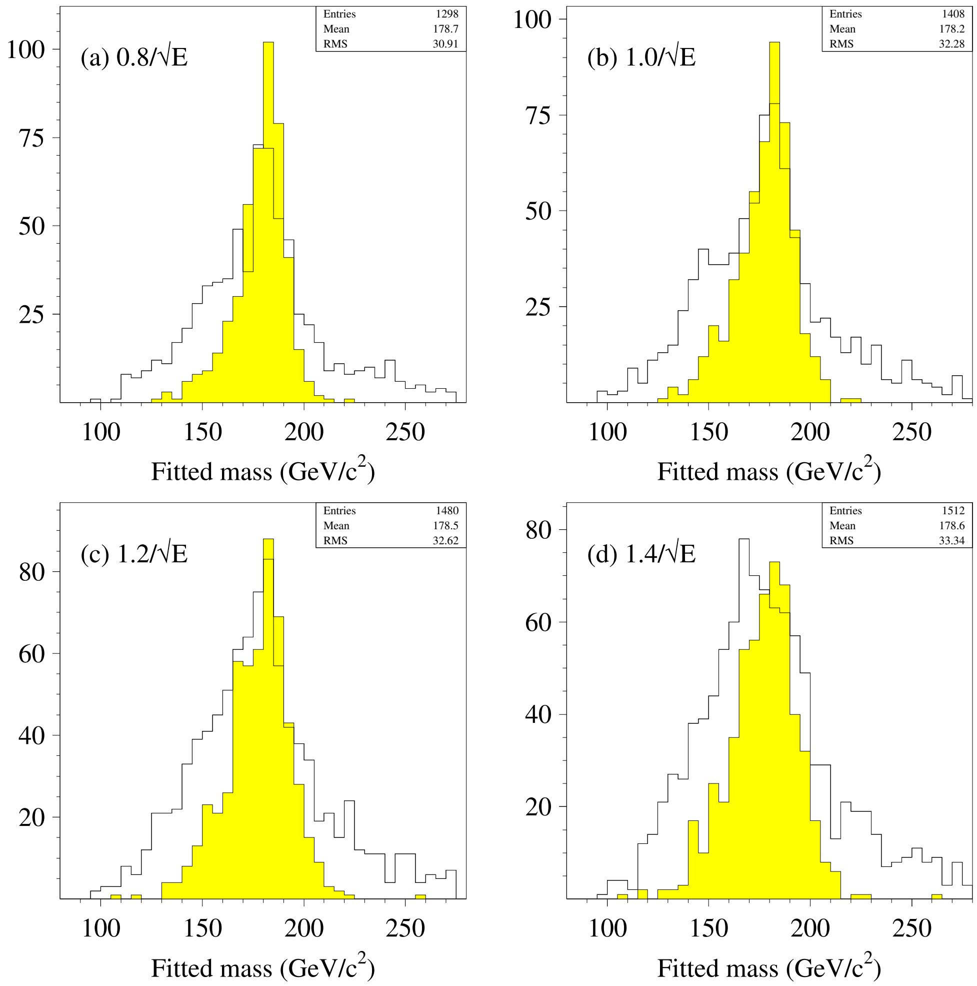

Figure 6.7: Fitted mass distributions for smeared $t\bar{t} \rightarrow e + \text{jets}$ ISAJET Monte Carlo with $m_t = 180\,\mathrm{GeV}/c^2$, for different jet smearings. (a) $0.80/\sqrt{E}$. (b) $1.00/\sqrt{E}$. (c) $1.20/\sqrt{E}$. (d) $1.40/\sqrt{E}$. Unshaded plots are the weighted average of the best three χ^2 solutions, shaded plots are the correct permutations.

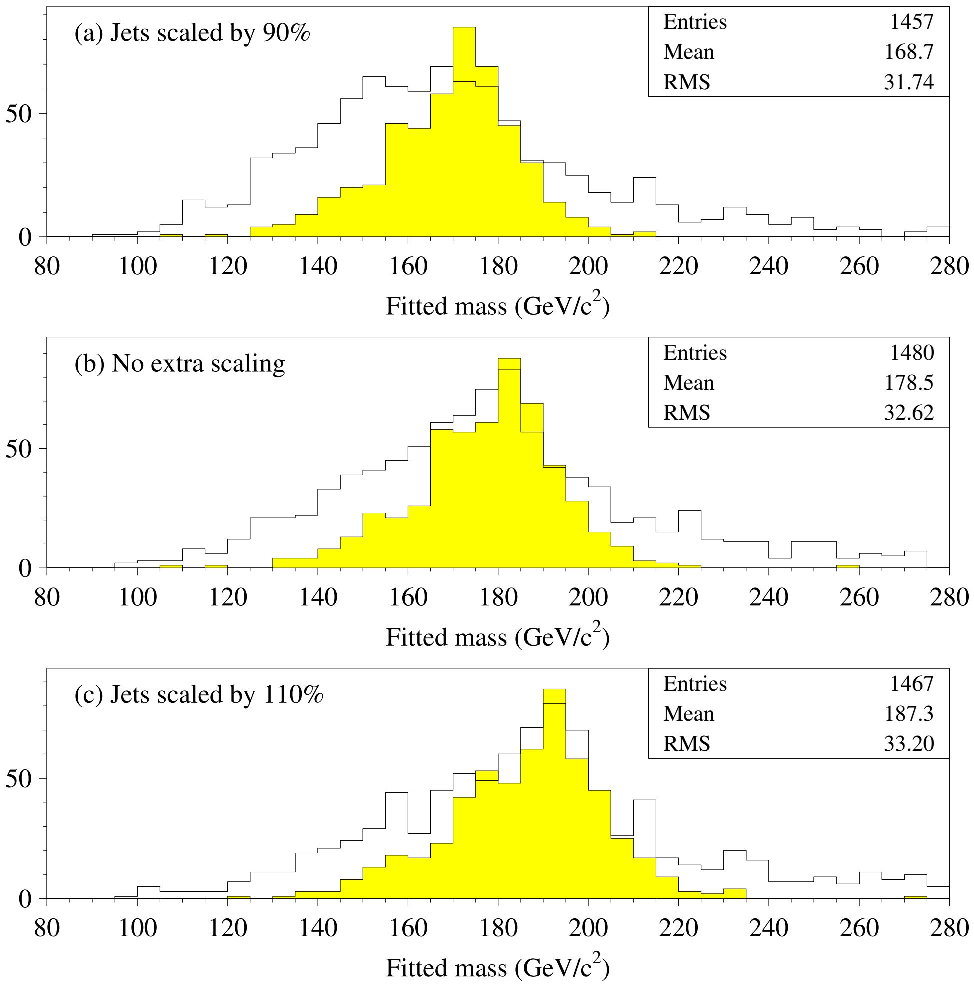

Figure 6.8: Fitted mass distributions for smeared $t\bar{t} \rightarrow e + \text{jets}$ ISAJET Monte Carlo with $m_t = 180\,\text{GeV}/c^2$, for different jet scalings. (a) Jets scaled by 90%. (b) Jets unscaled. (c) Jets scaled by 110%. Unshaded plots are the weighted average of the best three χ^2 solutions, shaded plots are the correct permutations.

6.5 Tests With Full Detector Simulation

The next step is to examine the results of the fitting algorithm for samples which have been through the full DØ detector simulation and reconstruction. All the Monte Carlo samples in this section have been subjected to the kinematic selection cuts described in Chapter 5.

The object resolutions which will be used for the fit are as follows.

$\frac{\sigma E(e)}{E(e)} = \frac{0.15}{\sqrt{E}} \oplus 0.03$	$\frac{\sigma k(\mu)}{k(\mu)} = \frac{0.01}{k} \oplus 0.2$	$\frac{\sigma E(\text{jet})}{E(\text{jet})} = \frac{0.82}{\sqrt{E}} \oplus 0.19$
$\sigma\phi(e) = 0.0060\,\text{rad}$	$\sigma\phi(\mu) = 0.0060\,\text{rad}$	$\sigma\phi(\text{jet}) = 0.035\,\text{rad}$
$\sigma\eta(e) = 0.0072$	$\sigma\eta(\mu) = 0.0072$	$\sigma\eta(\text{jet}) = 0.040$
$\sigma k_{T_x} = 12\,\text{GeV}$	$\sigma k_{T_y} = 12\,\text{GeV}$	

(6.12)

(Where E is measured in GeV and $k = 1/p$ is measured in GeV^{-1}.) Most of these values were determined by comparing the parton-level objects which were input to the detector simulation with the final objects output by the reconstruction program. The errors for the jet and electron energies are taken from [140]. The error for the muon momentum is taken from [43]. The results for the electron angular errors were reused for the muons. The large constant errors in the jet and electron energy resolutions above serve to account for the effects of radiation and the W width, which tend to spoil the kinematic constraints.

The muon momentum resolution in the Monte Carlo is known to be unrealistically good [47, p. 100]. To partially compensate for this, the momenta of high-p_T muons in the $\mu +$ jets Monte Carlo samples are smeared with the

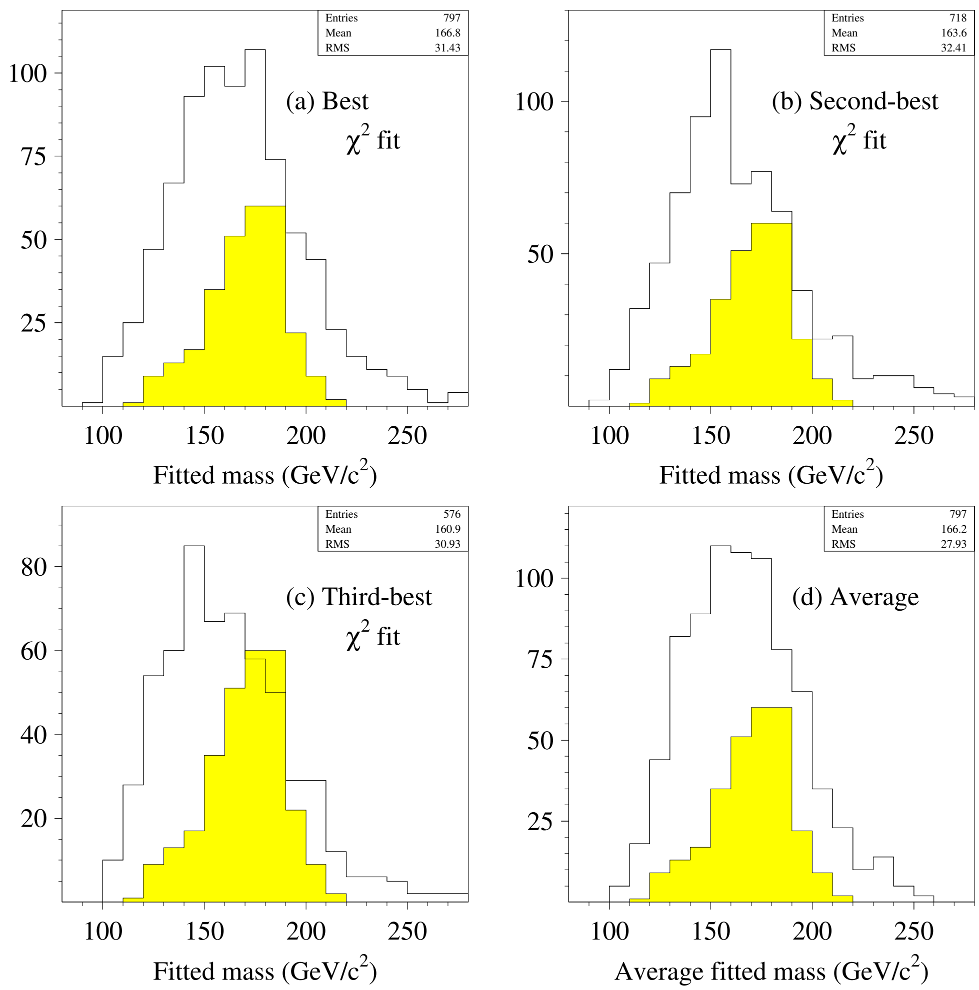

Figure 6.9: Fitted mass distributions for (a) best, (b) second-best, (c) third-best χ^2 solutions and (d) weighted average. For $t\bar{t} \to e + \text{jets}$ ISAJET Monte Carlo, with $m_t = 180\,\text{GeV}/c^2$. Shaded plots show the result for the correct jet permutation.

resolution given in (6.12).

The results of the fitter are shown for an ISAJET $t\bar{t} \rightarrow e+$jets Monte Carlo sample with $m_t = 180\,\mathrm{GeV}/c^2$ in Figure 6.9 (with full detector simulation and reconstruction). A χ^2 cut of $\chi^2 < 7$ was applied. As was seen with the parton-level tests, the averaging procedure reduces the tails of the distribution, while not introducing a significant bias. Also shown in Figure 6.10 is a comparison between the averaging procedure described above and an alternate procedure which consists of taking all solutions which satisfy the χ^2 cut (up to five per event) and plotting them with each one weighted by $e^{-\chi^2/2}$. This appears to be inferior to the averaging procedure.

Figure 6.11 shows the fit χ^2 distributions for the three lowest χ^2 jet permutations and for the correct permutation. The arrow shows the cut value. Note that the mean χ^2 for the correct jet permutation is close to 2, as expected for a 2C fit. However, this agreement was to some extent engineered by the inclusion of the large constant errors in the energy resolutions.

Figure 6.12 shows the fit results for all four lepton + jets channels. Compared to the $e+$jets channels, the $\mu+$jets channels show no additional biases, but are somewhat wider, due to the poor muon momentum resolution. The tagged channels are offset about 5–10 GeV/c^2 higher than the untagged channels; this is approximately independent of the input top mass. This is due to the additional corrections made for tagged jets. The resolution for the tagged channels is also slightly worse than for the untagged channels.

In the previous figure, the b-tag was enforced for the tagged channels, i.e., only jet permutations in which the tagged jet was used as a b were fit.

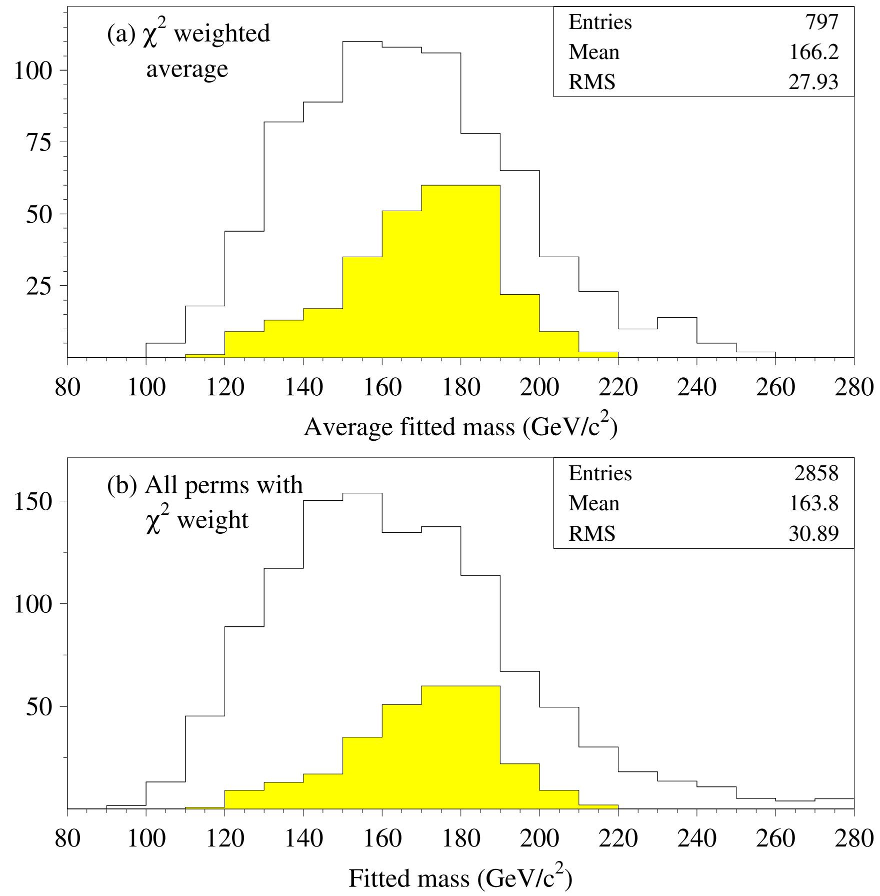

Figure 6.10: Comparison of (a) χ^2 weighted average of best three solutions, and (b) all solutions plotted, each one with a χ^2 weight. For $t\bar{t} \to e + \text{jets}$ ISAJET Monte Carlo, with $m_t = 180\,\text{GeV}/c^2$. Shaded plots show the result for the correct jet permutation.

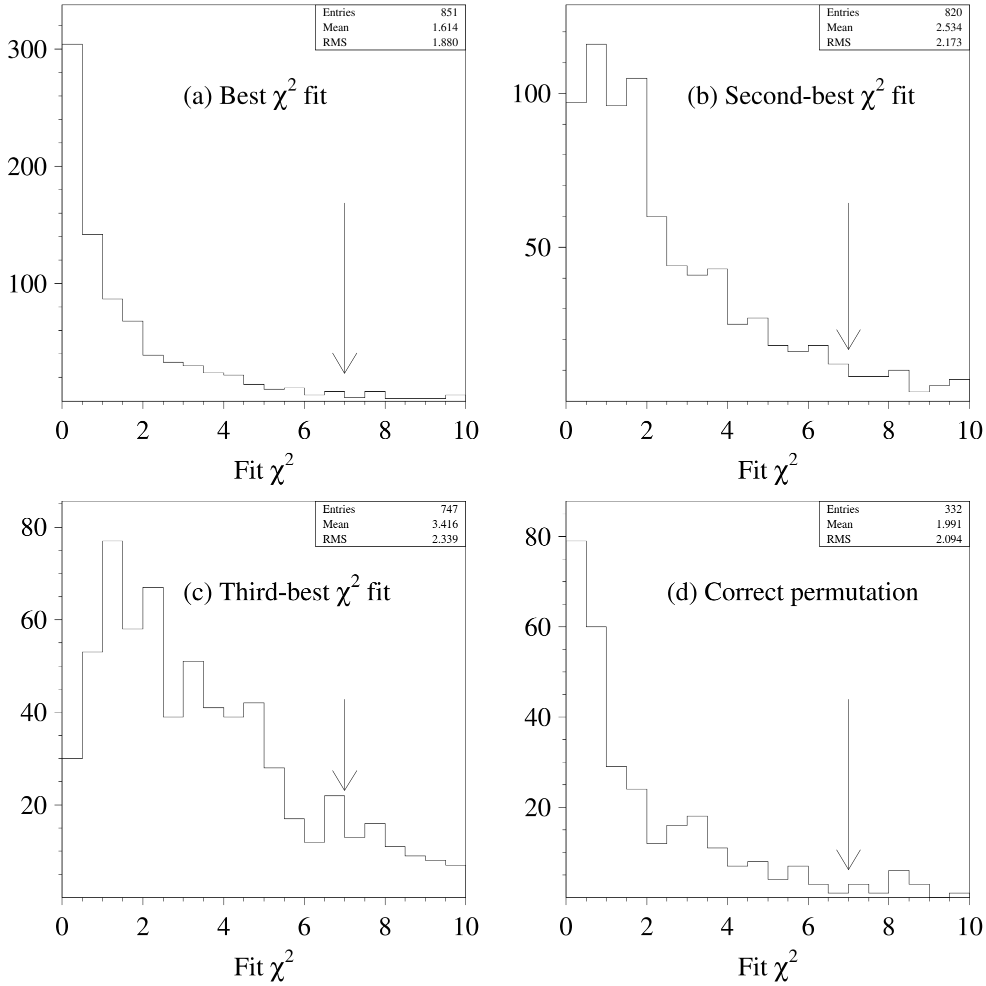

Figure 6.11: Fit χ^2 distributions for (a) best, (b) second-best, and (c) third-best χ^2 solutions and (d) the correct jet permutation. For $t\bar{t} \to e+\text{jets}$ ISAJET Monte Carlo, with $m_t = 180\,\text{GeV}/c^2$. The arrow shows the cut value.

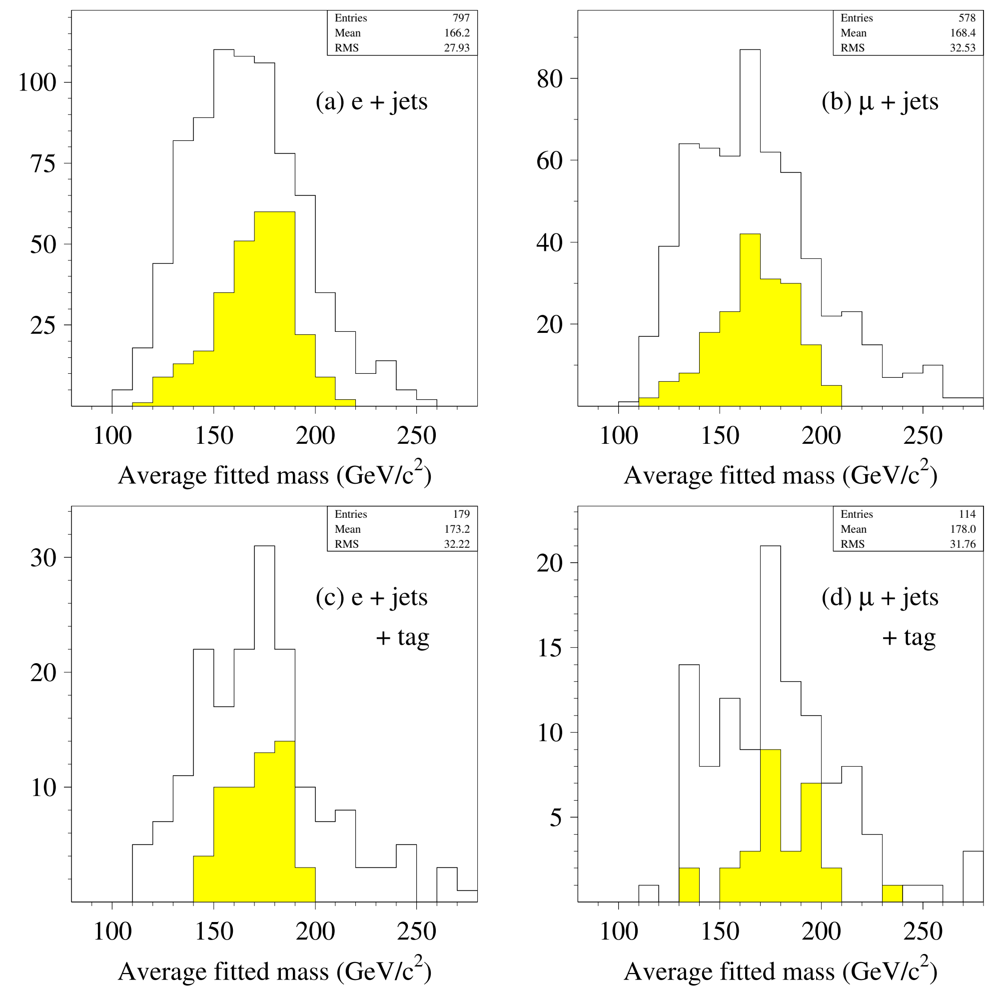

Figure 6.12: Fitted mass distributions for $t\bar{t}$ ISAJET Monte Carlo, with $m_t = 180\,\mathrm{GeV}/c^2$. For (a) e+jets, (b) μ+jets, (c) e+jets+tag, and (d) μ+jets+tag. Muon tags are enforced in the tagged channels. Shaded plots show the result for the correct jet permutation.

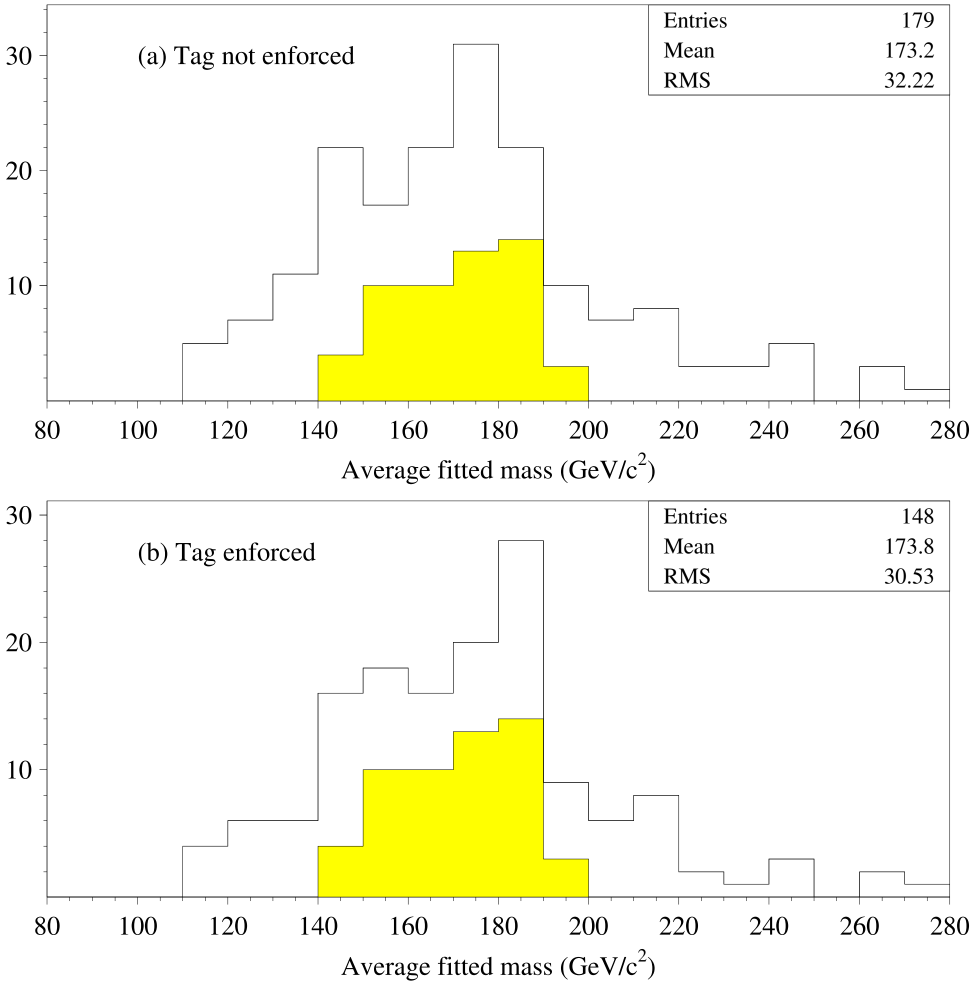

Figure 6.13: Fitted mass distributions, for the $e + \text{jets} + \text{tag}$ channel (a) with and (b) without enforcing b-tagging. For $t\bar{t}$ ISAJET Monte Carlo, with $m_t = 180\,\text{GeV}/c^2$. Shaded plots show the result for the correct jet permutation.

The effect of enforcing the tag is shown in Figure 6.13, which shows the same sample fit both with and without the tagging requirement. As can be seen, the difference is fairly small.

Figure 6.14 shows how the fitted mass distribution varies with the number of jets in the event. Looking at the RMS values, the degradation is surprisingly slow with increasing multiplicity.

In the previous figures, only the top four jets were used in the fit, no matter what the jet multiplicity in the event was. One can also consider trying to use additional jets, as discussed in Section 6.3.2. The result of doing so, without making any other alterations in the fitting procedure, is shown in Figure 6.15. Up to six jets were used, and all possible permutations were considered. However, although this procedure takes about an order of magnitude more computation time than always taking just the top four jets, the final result is not significantly better.

Another approach to try to deal with additional radiation is to increase the size of the jet cone. Figure 6.16 compares the results using the $R = 0.3$ jet cone to those obtained with a $R = 0.5$ cone. As can be seen, the results from the larger jet cone are somewhat inferior to those with the $R = 0.3$ cone. The caveat here is that the full set of out-of-cone corrections was not available for the $R = 0.5$ cone; however, the corrections one would make for that cone size are small [137].

Figure 6.17 shows the result of varying the jet scale up or down by the 10% error mentioned in Section 6.2.1. This translates into a change in the mean fit mass of about $9\,\mathrm{GeV}/c^2$ or $\approx 5\%$.

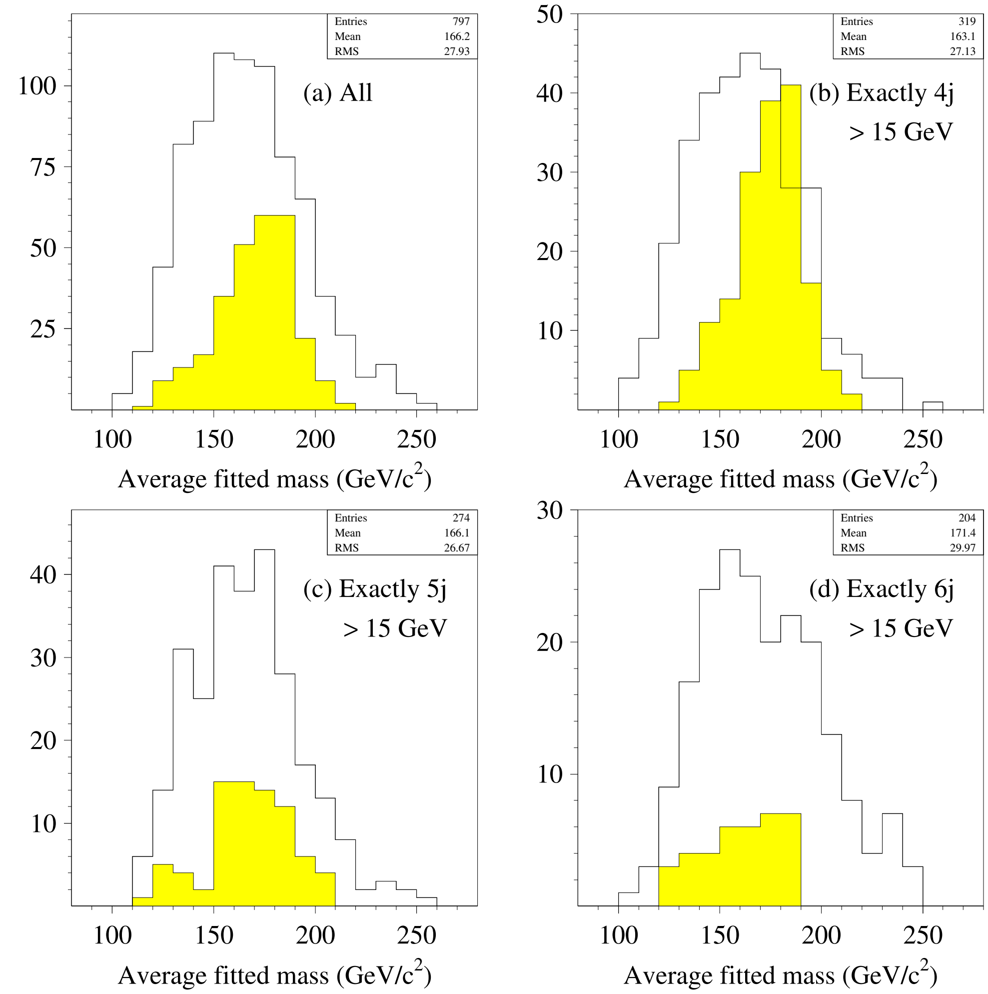

Figure 6.14: Fitted mass distributions for different jet multiplicities. (a) All multiplicities, (b) exactly four jets, (c) exactly five jets, and (d) exactly six jets. For $t\bar{t}$ ISAJET Monte Carlo, with $m_t = 180\,\mathrm{GeV}/c^2$ in the $e+$jets channel. Shaded plots show the result for the correct jet permutation.

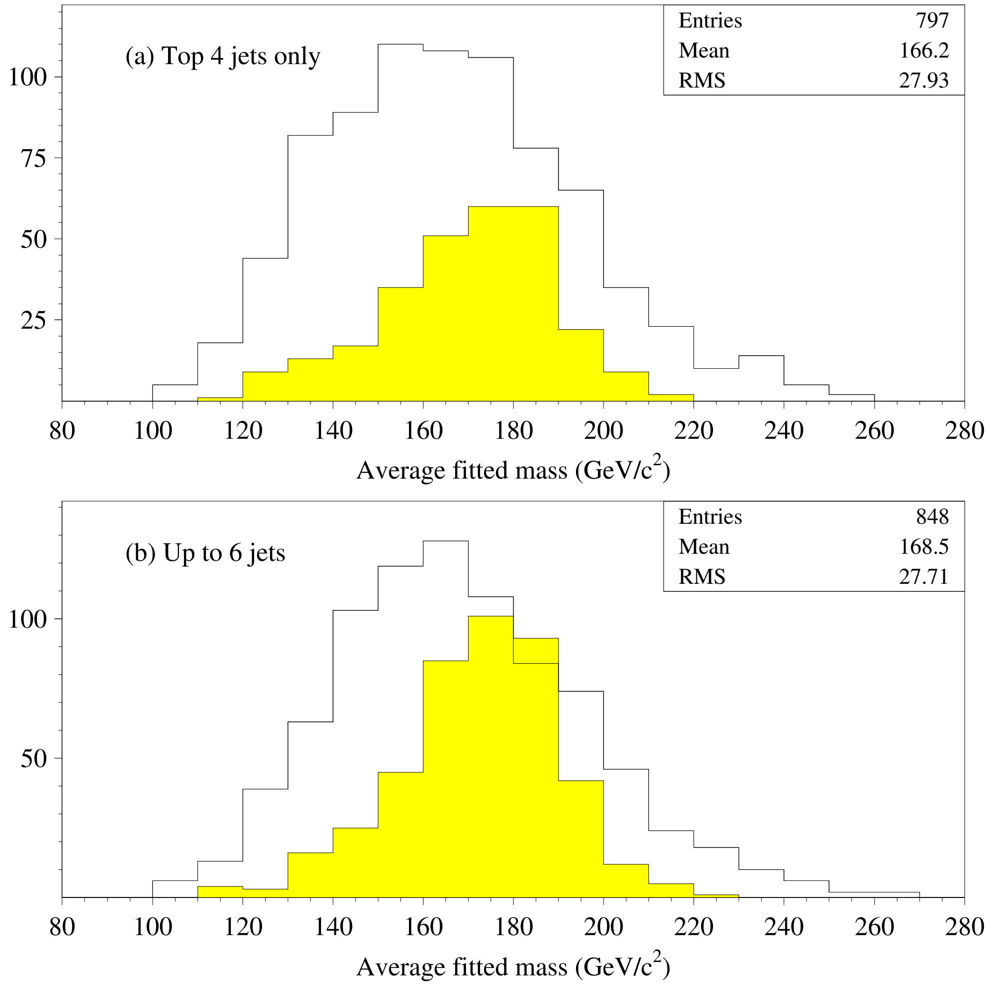

Figure 6.15: Fitted mass distributions for the $t\bar{t} \rightarrow e + \text{jets}$ channel using (a) only the top four jets and (b) up to six jets. For $t\bar{t}$ ISAJET Monte Carlo, with $m_t = 180\,\text{GeV}/c^2$. Shaded plots show the result for the correct jet permutation.

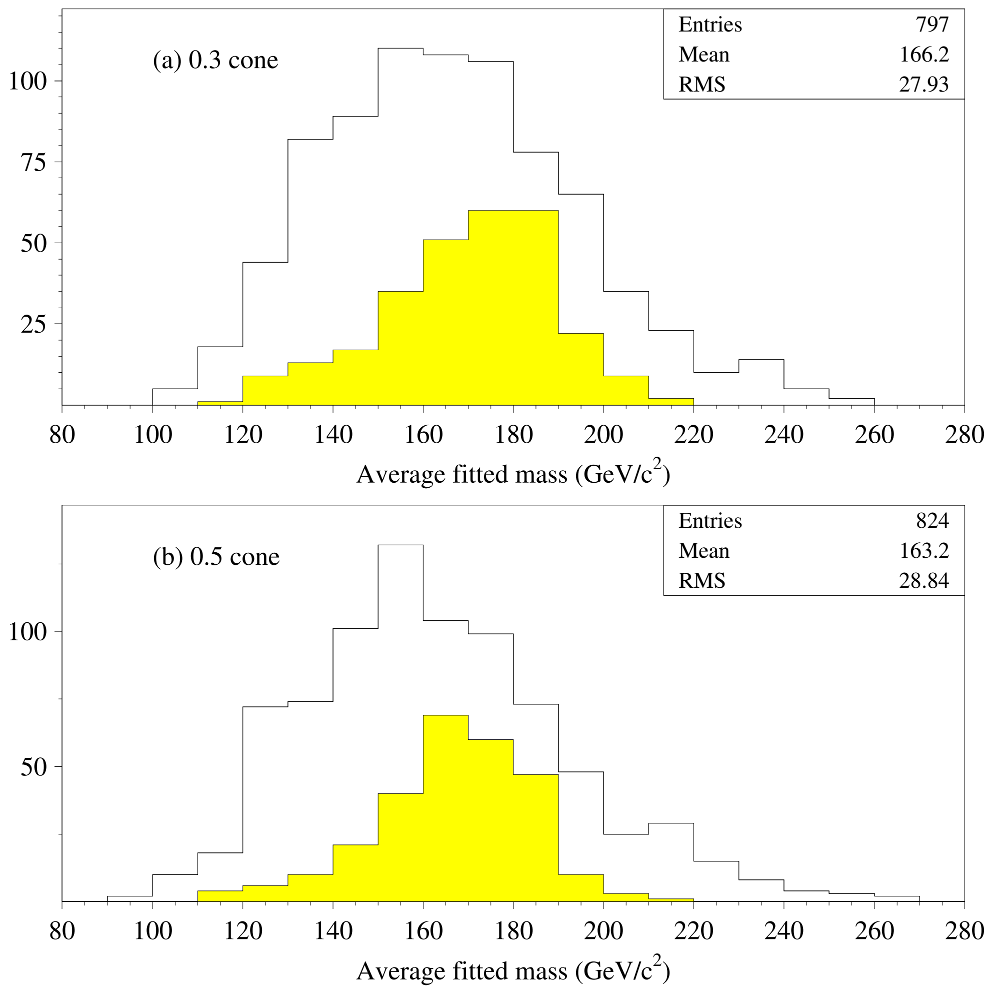

Figure 6.16: Fitted mass distributions for the $t\bar{t} \to e + \text{jets}$ channel using (a) $R = 0.3$ cone jets and (b) $R = 0.5$ cone jets. For ISAJET Monte Carlo, with $m_t = 180\,\text{GeV}/c^2$. Shaded plots show the result for the correct jet permutation.

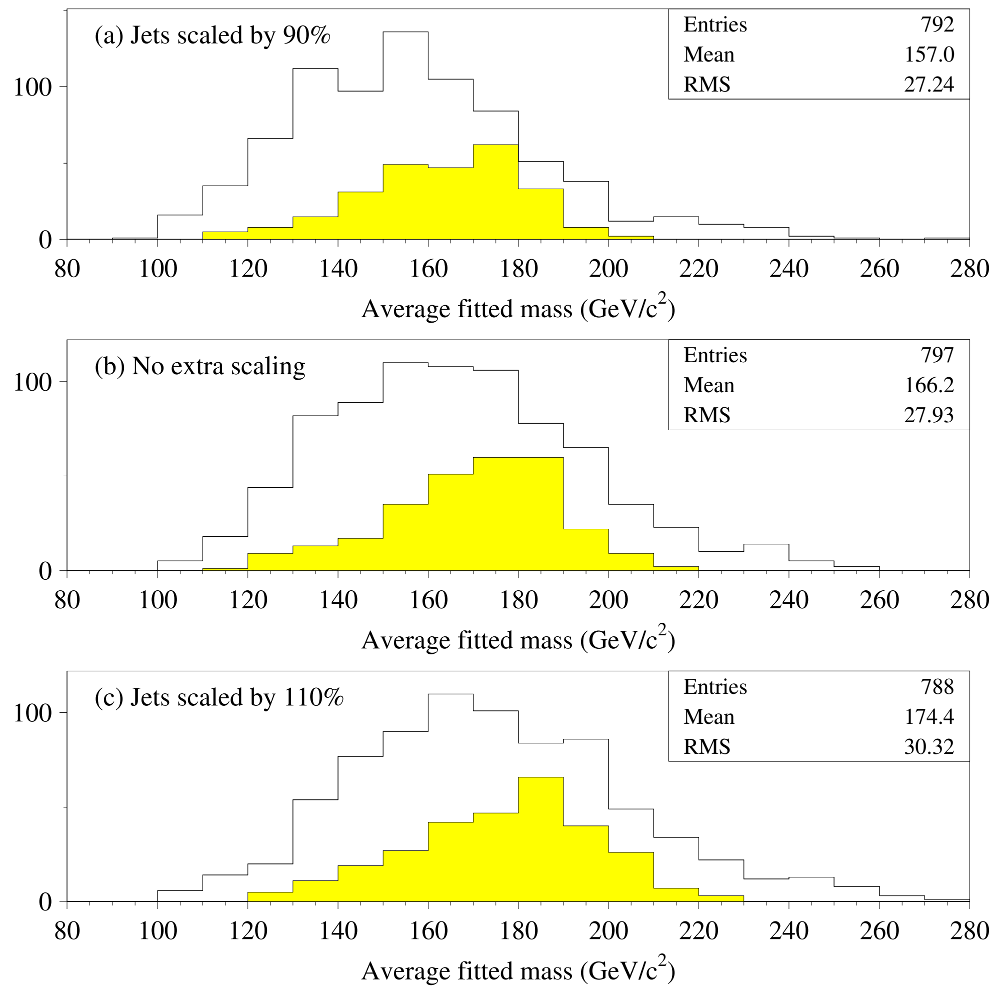

Figure 6.17: Fitted mass distributions for the $t\bar{t} \to e + \text{jets}$ channel with jets scaled by (a) 90%, (b) 100%, and (c) 110%. For $t\bar{t}$ ISAJET Monte Carlo, with $m_t = 180\,\text{GeV}/c^2$. Shaded plots show the result for the correct jet permutation.

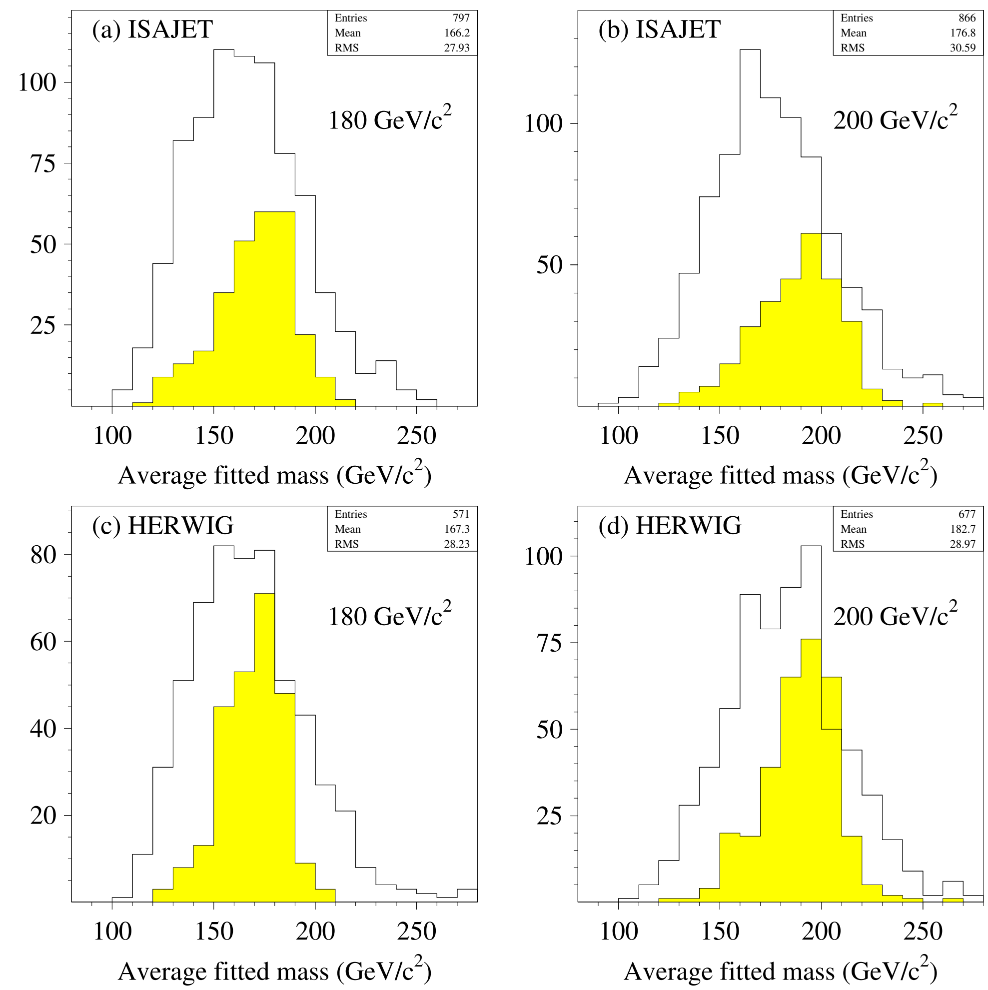

Figure 6.18: Fitted mass distributions for the $t\bar{t} \rightarrow e + \text{jets}$ channel for (a) $t\bar{t}$ ISAJET with $m_t = 180\,\text{GeV}/c^2$, (b) $t\bar{t}$ ISAJET with $m_t = 200\,\text{GeV}/c^2$, (c) $t\bar{t}$ HERWIG with $m_t = 180\,\text{GeV}/c^2$, and (d) $t\bar{t}$ HERWIG with $m_t = 200\,\text{GeV}/c^2$. Shaded plots show the result for the correct jet permutation.

Besides ISAJET, another popular Monte Carlo event generator is HERWIG. The results from the two are compared in Figure 6.18. Empirically, HERWIG is seen to produce somewhat less radiation than ISAJET does. This is reflected in the fact that it is more likely to find the correct jet permutation with HERWIG. This can be seen in the figure and also in the numbers in Table 6.1. As for the shape of the fitted mass distribution, there is not much difference between ISAJET and HERWIG for a top mass of 180 GeV/c^2. However, at 200 GeV/c^2, the difference is much more pronounced: the HERWIG distribution has somewhat less bias, and is also slightly narrower. (It is interesting to note that there is now some evidence that HERWIG underestimates the amount of radiation which is produced [138].)

Table 6.1 also shows that the efficiency for finding the correct permutation goes up slightly with increasing top mass. By contrast, these efficiencies do not change appreciably when the kinematic cuts ($\mathcal{A}$ and H_T) are changed.

So far, all the plots which have been shown have used the loose cuts. Figure 6.19 compares those results with those obtained when either the standard cuts or no $\mathcal{A}$, H_T cuts are used, for several top masses and the VECBOS W+jets background. The loose cuts, which consist of only a relaxed aplanarity cut, are seen not to change the shapes of the distributions appreciably. The standard cuts, on the other hand, add a fairly high H_T cut and bias the fitted mass distributions for low input masses significantly upwards. The background is also biased upwards. This bias is not large, however, for input top masses above about 180 GeV/c^2.

For the final set of fitted mass distributions, the results from all channels

	ISAJET		HERWIG	
Top mass (GeV/c^2)	160	200	160	200
(a) Probability of having the correct four partons as the top four jets	$39 \pm 2\%$	$42 \pm 2\%$	$47 \pm 3\%$	$52 \pm 2\%$
(b) Given (a), probability of having a good fit for the correct permutation	$85 \pm 5\%$	$78 \pm 4\%$	$89 \pm 5\%$	$85 \pm 4\%$
(c) Given (b), probability of the correct fit having the lowest χ^2	$32 \pm 3\%$	$40 \pm 3\%$	$42 \pm 4\%$	$50 \pm 3\%$
(d) Given (b), probability of the correct fit being in the best three fits	$67 \pm 4\%$	$75 \pm 4\%$	$79 \pm 5\%$	$84 \pm 4\%$
Total chance of getting the correct permutation by picking the lowest χ^2	$11 \pm 1\%$	$13 \pm 1\%$	$18 \pm 2\%$	$22 \pm 2\%$
Total chance of getting the correct permutation in the best three fits	$22 \pm 2\%$	$25 \pm 1\%$	$33 \pm 2\%$	$37 \pm 2\%$

Table 6.1: Efficiencies for finding the correct jet permution, for ISAJET and HERWIG. From $t\bar{t} \rightarrow e + \text{jets}$ Monte Carlo. Errors are statistical only.

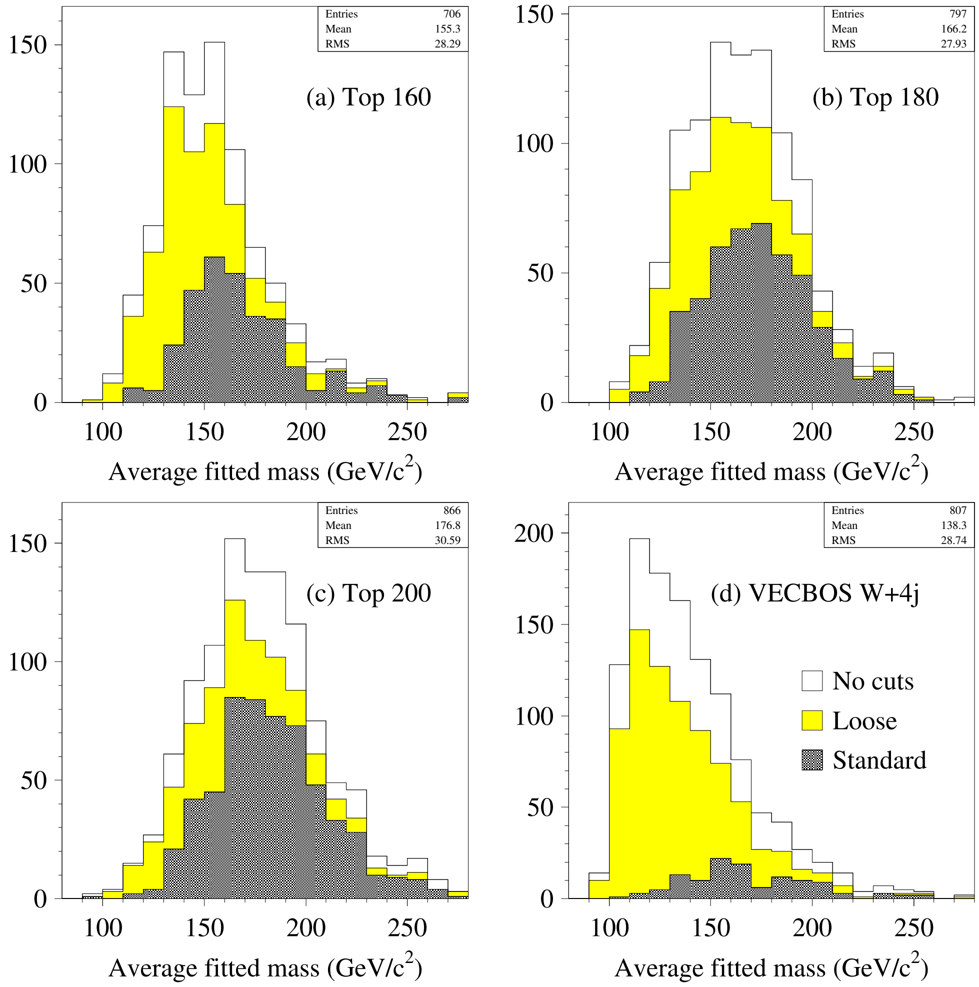

Figure 6.19: Fitted mass distributions for the e + jets channel using either no $\mathcal{A}$, H_T cuts (unshaded plot), loose cuts (lightly shaded plot), or standard cuts (dark plot) for (a) $m_t = 160\,\mathrm{GeV}/c^2$ ISAJET $t\bar{t}$ Monte Carlo, (b) $m_t = 180\,\mathrm{GeV}/c^2$ ISAJET $t\bar{t}$ Monte Carlo, (c) $m_t = 200\,\mathrm{GeV}/c^2$ ISAJET $t\bar{t}$ Monte Carlo, and (d) VECBOS W + jets Monte Carlo. Statistics reflect the loose cuts histogram.

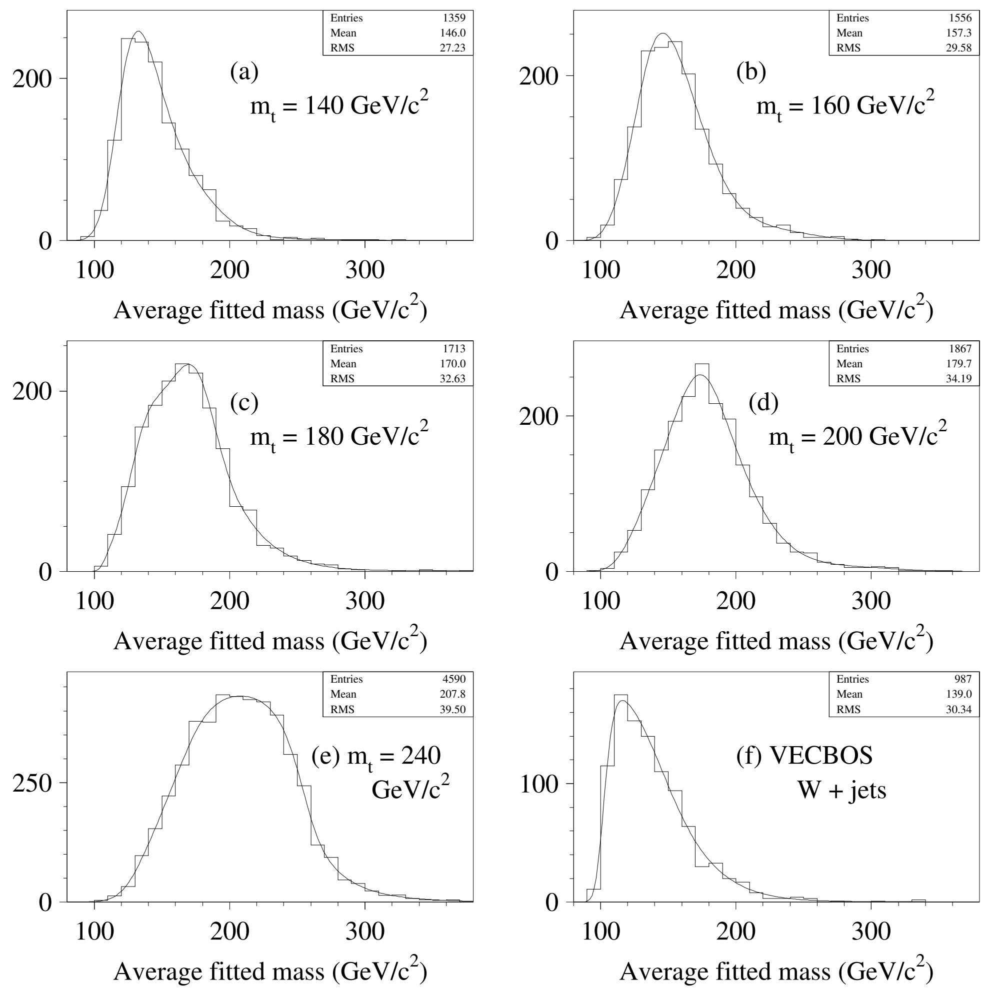

Figure 6.20: Final fitted mass distributions for all channels combined For loose cuts, using ISAJET. (a) $m_t = 140\,\mathrm{GeV}/c^2$, (b) $m_t = 160\,\mathrm{GeV}/c^2$, (c) $m_t = 180\,\mathrm{GeV}/c^2$, (d) $m_t = 200\,\mathrm{GeV}/c^2$, (e) $m_t = 240\,\mathrm{GeV}/c^2$, and (f) VECBOS $W +$ jets background.

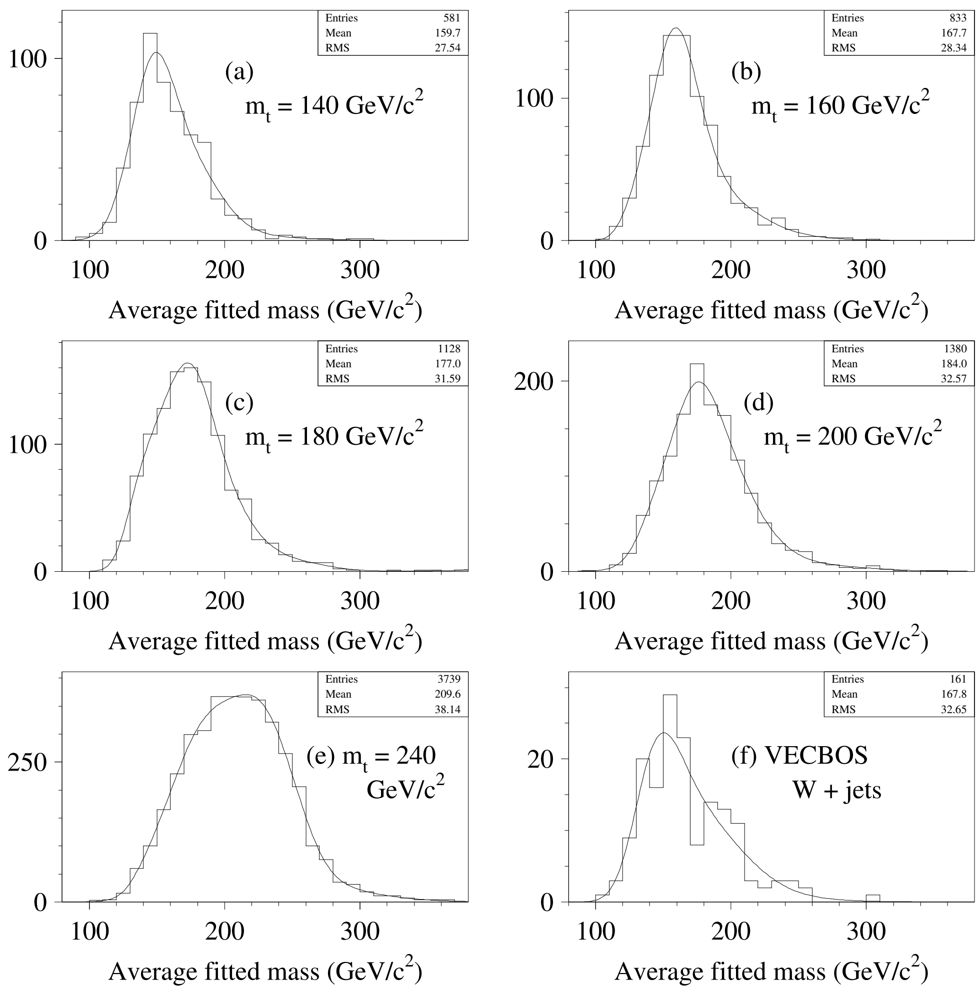

Figure 6.21: Final fitted mass distributions for all channels combined. For standard cuts, using ISAJET. (a) $m_t = 140\,\mathrm{GeV}/c^2$, (b) $m_t = 160\,\mathrm{GeV}/c^2$, (c) $m_t = 180\,\mathrm{GeV}/c^2$, (d) $m_t = 200\,\mathrm{GeV}/c^2$, (e) $m_t = 240\,\mathrm{GeV}/c^2$, and (f) VECBOS $W + \mathrm{jets}$ background.

are combined together, by simply adding together the appropriate Monte Carlo samples (with no additional weights; the samples were originally generated according to the appropriate branching ratios). Figures 6.20 and 6.21 show the results for all five top masses used as well as the VECBOS $W+$jets background, for both the loose and standard cuts. (There was no $\mu+$jets Monte Carlo for $m_t = 240\,\mathrm{GeV}/c^2$, so the $e+$jets sample was reused for the $\mu+$jets channel at that mass point.) Note that the lower mass tops have tails on the high side which bias them upwards, while the higher mass tops are biased downwards. If one plots the relation between the mean fitted mass and the input mass, one finds that it is close to linear, with a slope of about 0.6 with the loose cuts and 0.5 with the standard cuts (this is shown in Figure 6.22). The standard cuts have a smaller slope due to the larger biases present for small masses. This has the unfortunate consequence that any errors in the fitted masses will be inflated by approximately the inverse of this slope when converting to the final mass value.

For reference, the results are shown broken down by the individual channels in Figures 6.23, 6.24, 6.25, and 6.26. Note that the available Monte Carlo statistics are rather poor for the tagged channels; this is the major motivation for combining all channels together.

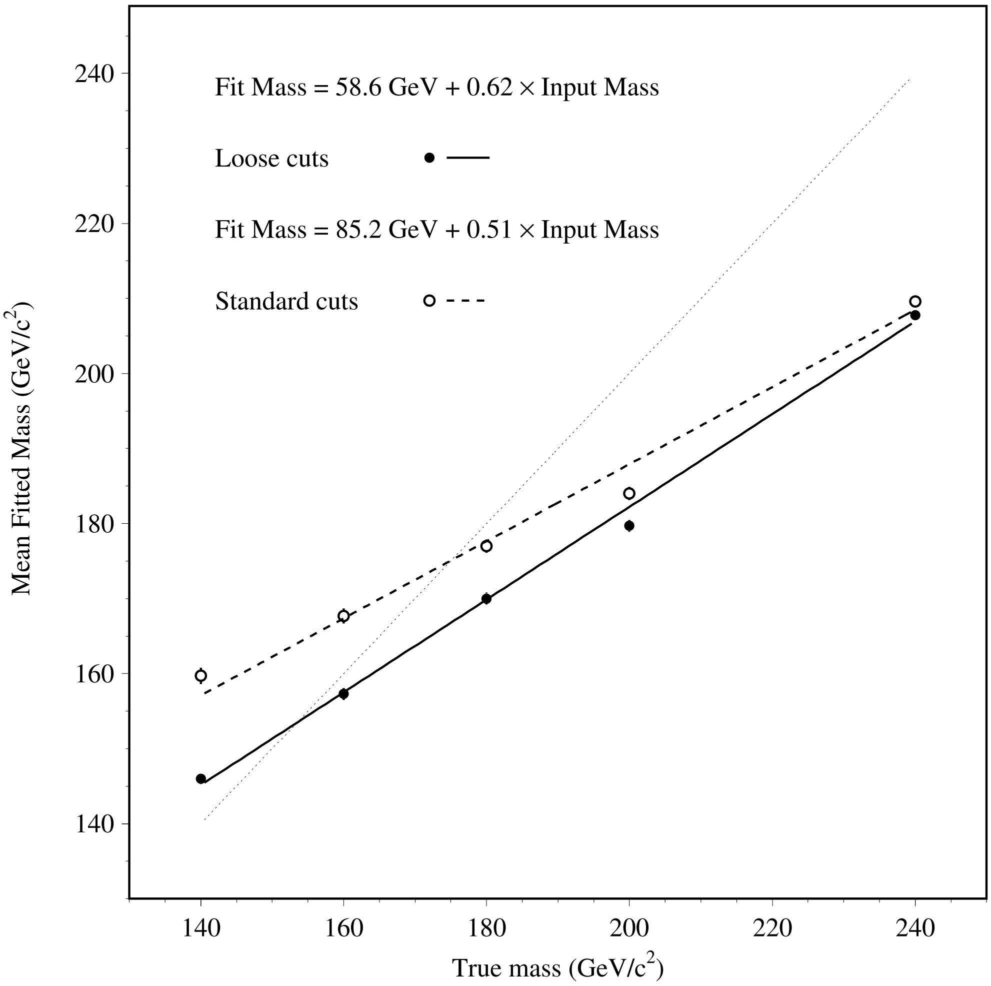

Figure 6.22: Mean fitted mass as a function of input mass for loose and tight cuts. From $t\bar{t}$ ISAJET Monte Carlo with all channels combined. The dotted line is drawn along the diagonal for comparison.

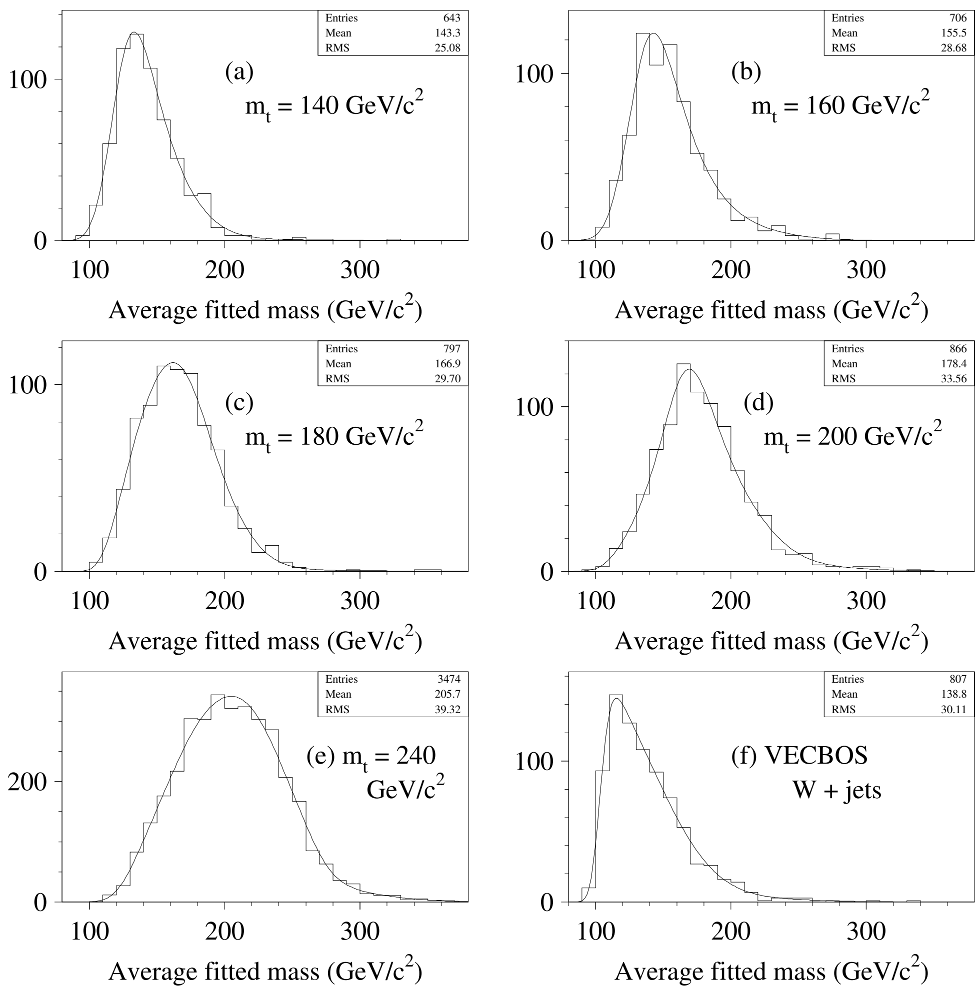

Figure 6.23: Final fitted mass distributions for e + jets channel. For loose cuts, using ISAJET. (a) $m_t = 140\,\mathrm{GeV}/c^2$, (b) $m_t = 160\,\mathrm{GeV}/c^2$, (c) $m_t = 180\,\mathrm{GeV}/c^2$, (d) $m_t = 200\,\mathrm{GeV}/c^2$, (e) $m_t = 240\,\mathrm{GeV}/c^2$, and (f) VECBOS $W +$ jets background.

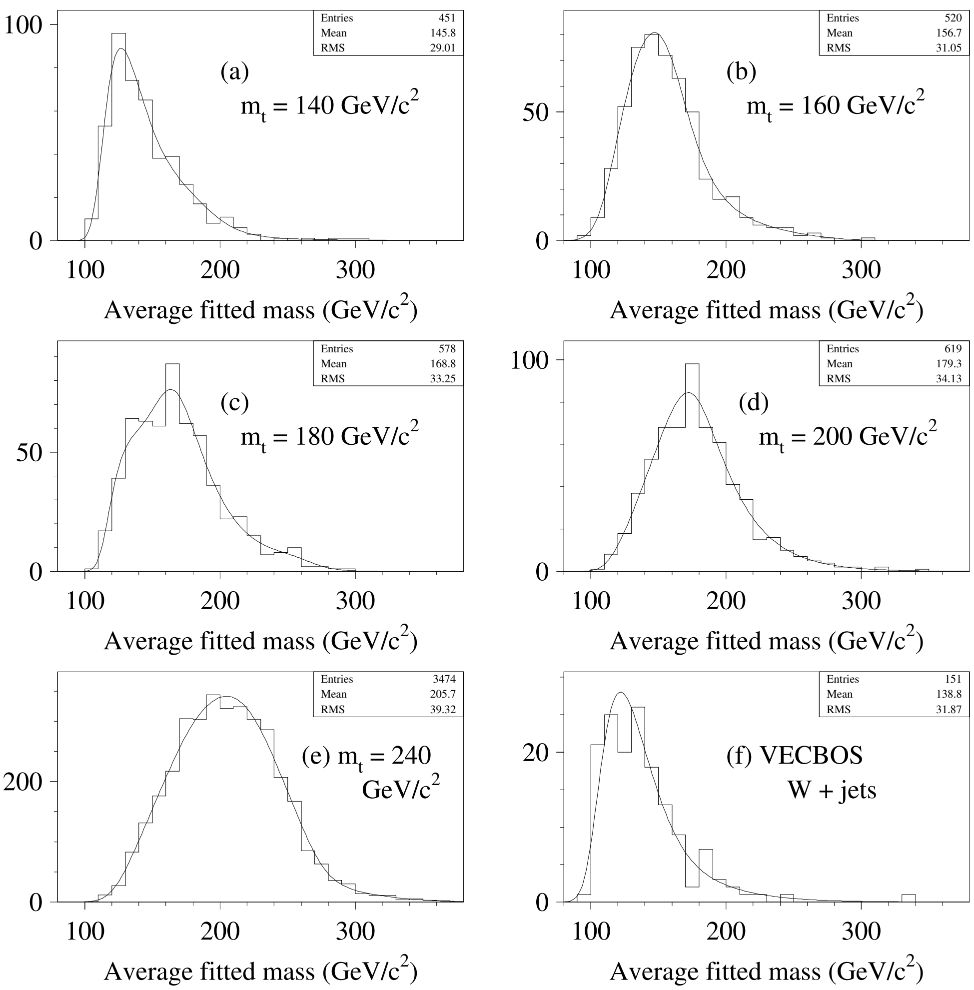

Figure 6.24: Final fitted mass distributions for μ + jets channel. For loose cuts, using ISAJET. (a) $m_t = 140\,\mathrm{GeV}/c^2$, (b) $m_t = 160\,\mathrm{GeV}/c^2$, (c) $m_t = 180\,\mathrm{GeV}/c^2$, (d) $m_t = 200\,\mathrm{GeV}/c^2$, (e) $m_t = 240\,\mathrm{GeV}/c^2$, and (f) VECBOS $W +$ jets background.

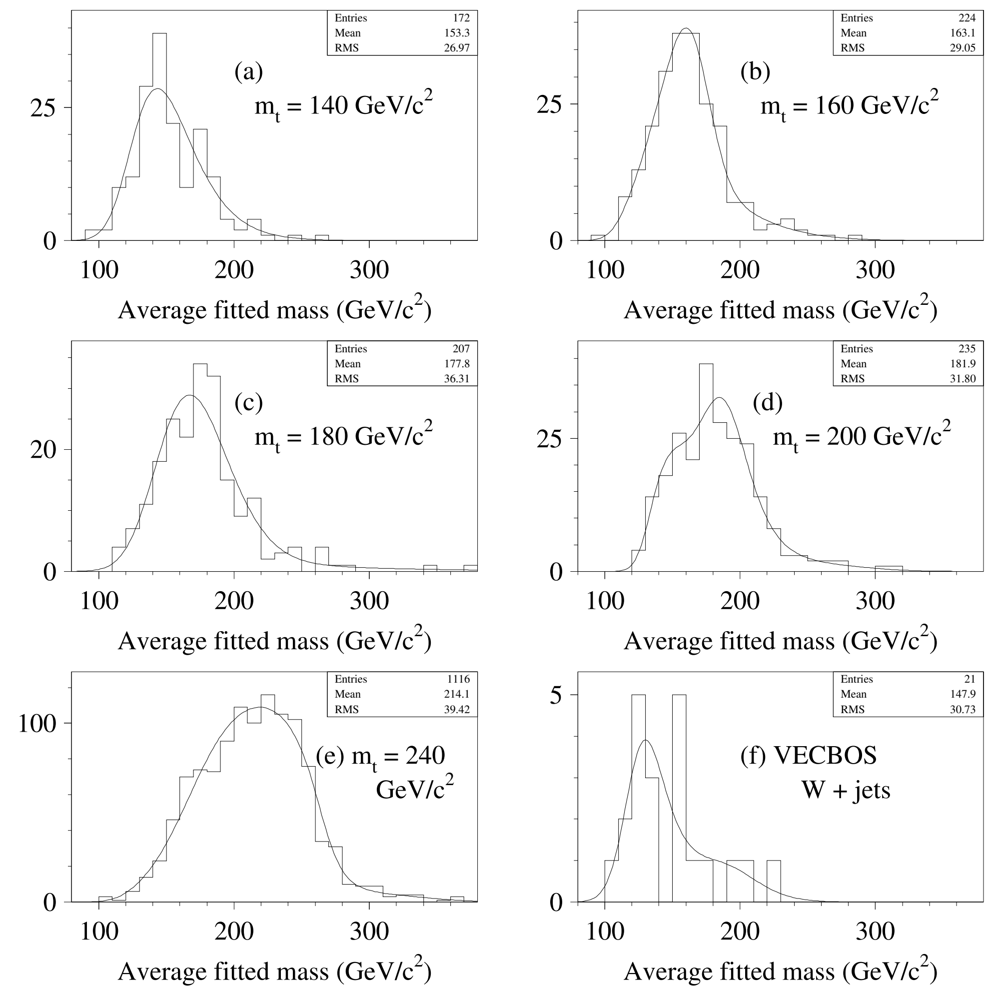

Figure 6.25: Final fitted mass distributions for $e+$jets/μ channel. For loose cuts, using ISAJET. (a) $m_t = 140\,\mathrm{GeV}/c^2$, (b) $m_t = 160\,\mathrm{GeV}/c^2$, (c) $m_t = 180\,\mathrm{GeV}/c^2$, (d) $m_t = 200\,\mathrm{GeV}/c^2$, (e) $m_t = 240\,\mathrm{GeV}/c^2$, and (f) VECBOS $W+$ jets background.

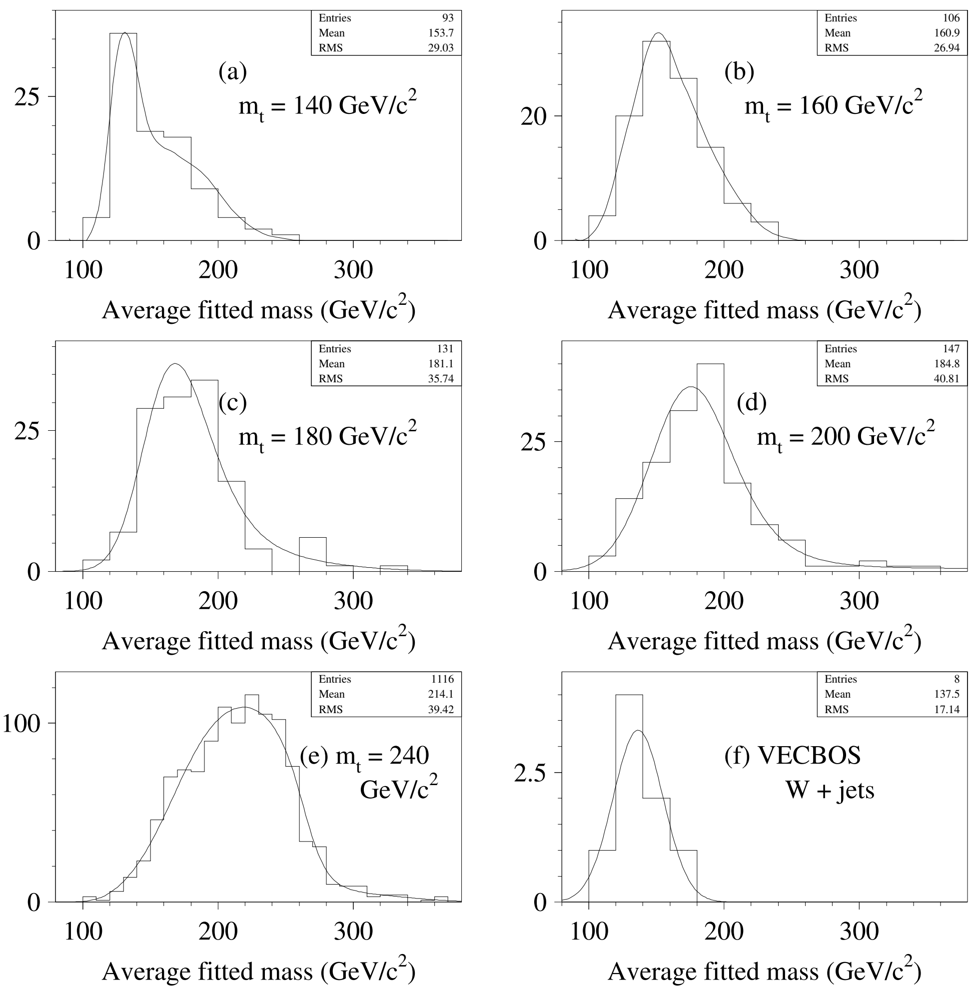

Figure 6.26: Final fitted mass distributions for $\mu + \text{jets}/\mu$ channel. For loose cuts, using ISAJET. (a) $m_t = 140\,\text{GeV}/c^2$, (b) $m_t = 160\,\text{GeV}/c^2$, (c) $m_t = 180\,\text{GeV}/c^2$, (d) $m_t = 200\,\text{GeV}/c^2$, (e) $m_t = 240\,\text{GeV}/c^2$, and (f) VECBOS $W +$ jets background.

6.6 Summary

Figure 6.27 summarizes the effects which contribute to the broadening of the fitted mass distributions. Figure 6.27(a) shows the result from an unsmeared, parton-level Monte Carlo with only the correct permutation chosen. The major factors contributing to the width here are final-state radiation which is lost by choosing only the top four jets and (to a lesser extent) the W widths and initial state radiation which is merged into final-state pjets. The width this plot is already half of the width of the final distribution (Figure 6.27(d)). Figures 6.27(b) and (c) show what happens when parton smearing is turned on (using the same resolutions as in Section 6.4) and when the full detector simulation is used. Both of these increase the width of the distribution, but only by a few GeV/c^2 each. Note, however, that the result from the full detector simulation is shifted down somewhat; this is probably due to reconstruction inefficiencies for low-energy jets. Finally, Figure 6.27(d) shows the result when all jet permutations are considered, not just the correct one. This step shows a large increase in the width of the distribution. Taken together, these plots imply that the major contributions to the widths of the fitted mass distributions come from radiation and from the jet combinatorics and not from the measurement errors on the jets themselves.

Recall that the slope seen in the relation between the input mass and the mean fitted mass was about 0.62. If one makes the same calculation using only the correct jet permutations, the result is a slope of about 0.94; if one does it using only jet permutations which do not assign the correct jets to the correct

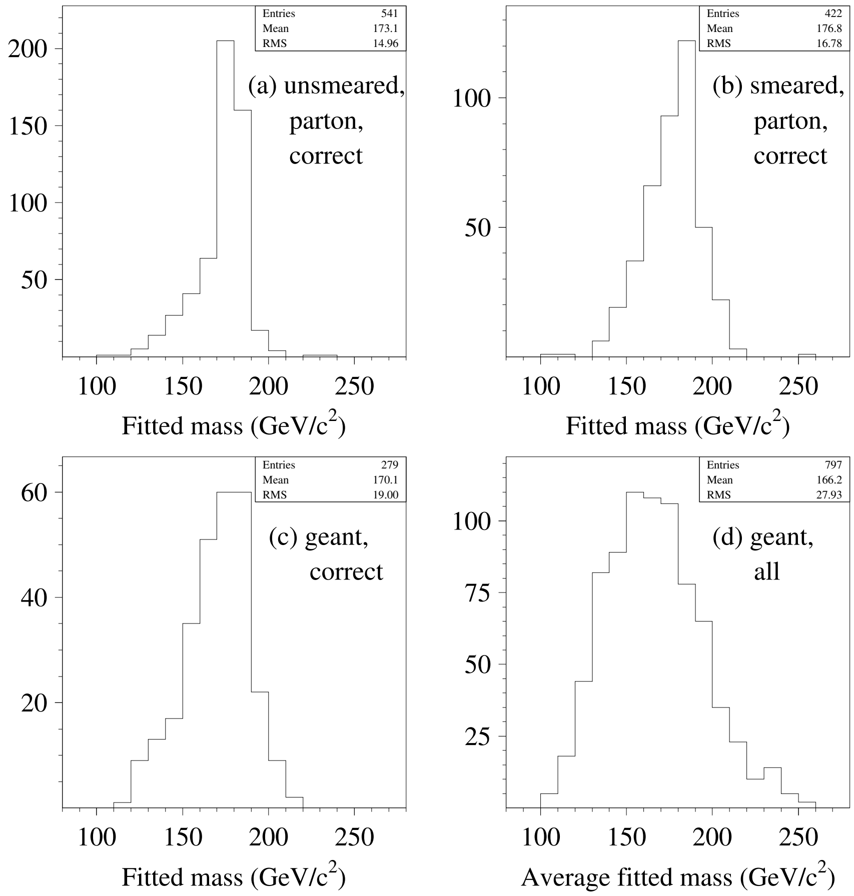

Figure 6.27: Fitted mass distributions for $t\bar{t} \to e + \text{jets}$ ISAJET Monte Carlo, with $m_t = 180\,\mathrm{GeV}/c^2$. (a) Parton-level, unsmeared, correct permutation. (b) Parton-level, smeared, correct permutation. (c) Detector simulation, correct permutation. (d) Detector simulation, average of best three permutations.

tops, the resulting slope is about 0.56. This indicates that the shallowness of this slope is another effect of the jet combinatorics.

These results imply that a possible avenue for improving the resolutions is to try to develop methods for identifying initial and final state radiation.